Engineering Structures 176 (2018) 585–605

Contents lists available at ScienceDirect

Engineering Structures

journal homepage: www.elsevier.com/locate/engstruct

Prestressed CFRP-strengthening and long-term wireless monitoring of an old roadway metallic bridge

Elyas Ghafoori[a,b,*], Ardalan Hosseini[a,c], Riadh Al-Mahaidi[b], Xiao-Ling Zhao[d], Masoud Motavalli[a,d]

[a] Empa, Structural Engineering Research Laboratory, Swiss Federal Laboratories for Materials Science and Technology, Duebendorf 8600, Switzerland
[b] Smart Structures Laboratory, Swinburne University of Technology, Hawthorn VIC 3122, Melbourne, Australia
[c] Resilient Steel Structures Laboratory, Swiss Federal Institute of Technology Lausanne (EPFL), Lausanne 1015, Switzerland
[d] Department of Civil Engineering, Monash University, Clayton 3800, Australia

ARTICLE INFO

Keywords:
Prestressed CFRP plates
Metallic bridges
Wireless sensor network (WSN) monitoring
Long-term structural health monitoring (SHM)

ABSTRACT

This paper presents an application of prestressed carbon fiber-reinforced polymer (CFRP) plates for the strengthening of metallic girders of a roadway bridge in Melbourne, Australia. The study also describes the application of a wireless sensor network (WSN) system for long-term structural monitoring of the retrofitted bridge girders. A flat prestressed unbonded retrofit (FPUR) system was developed to apply prestressed CFRP plates to the steel girders of the Diamond Creek Bridge (122 years old), which is subjected to daily passenger and heavy vehicles. The first section explains the results of sets of static and fatigue tests performed in the laboratory to examine the efficiency of the proposed FPUR system prior to its installation on the bridge. The second section presents details of different aspects of the CFRP strengthening of the bridge girders, fatigue design criteria, and layouts for short- and long-term monitoring. For the short-term measurements, the bridge was loaded with a 42.5-ton semi-trailer before and after strengthening. The CFRP plates were prestressed up to approximately 980 MPa (≈38% of the CFRP ultimate tensile strength), which resulted in about 50% reduction in the maximum tensile stress in the bridge girders. The third section discusses the development, installation, and preliminary results of the WSN system used to monitor the pre-stress level in the CFRP plates. The results of the short- and long-term measurements in this study show that the FPUR system is very effective for flexural and fatigue strengthening of bridge girders. Finally, a set of recommendations for long-term structural monitoring is provided.

1. Introduction

Metallic members are used in different types of structures and various engineering domains. In the civil engineering domain, they are used in offshore structures, communication towers, and railway and roadway bridges; in the mechanical engineering domain, they are used in shafts, mining equipment, pipelines, trams, and trains; and in the aerospace engineering domain, in aircraft, ships, and helicopters. Although these metallic structures belong to different engineering disciplines, aging degradation and fatigue cracking are common problems for all of them. It is known that fatigue is responsible for the failure of the majority of metallic structures.

In the civil engineering domain in Europe, nearly 30% of the metallic bridges are older than 100 years and nearly 70% of them are more than 50 years old [1]. A similar picture has been reported for the state of the bridge infrastructure in the USA [2], Australia [3], and Japan [4]. Aging of metallic bridges is a worldwide problem, which needs more attention. Therefore, there is a need for the development of different and versatile retrofitting systems.

Carbon fiber-reinforced polymer (CFRP), a light material with a wide range of strengths and Young's moduli, has been used for strengthening concrete and steel members. CFRP materials have high corrosion and fatigue resistance [5]. Several studies have proven the effectiveness of using CFRP materials for flexural (e.g., [6,7]) and fatigue (e.g., [8–10]) strengthening of steel members.

Most existing studies on this topic have used a bonded retrofit (BR) system to attach the CFRP material to steel substrates (e.g., [11–16]). Despite extensive laboratory studies of BR systems, in practice, the CFRP strengthening of metallic bridges has not advanced by much. The main two reasons for the limited use of bonded CFRP reinforcement in practice can be attributed to [17]:

(I) concerns related to the long-term performance of CFRP-to-steel bonded joints under special environmental conditions (e.g.,

* Corresponding author at: Empa, Swiss Federal Laboratories for Materials Science and Technology, Duebendorf 8600, Switzerland.
E-mail address: elyas.ghafoori@empa.ch (E. Ghafoori).

https://doi.org/10.1016/j.engstruct.2018.09.042
Received 20 June 2018; Received in revised form 10 September 2018; Accepted 14 September 2018

elevated or sub-zero temperatures, humidity, ultraviolet light, etc.),
(II) as the strengthening of metallic structures using non-prestressed CFRP does not greatly increase the stiffness of members, the benefits of using non-prestressed CFRP to increase the serviceability limits of metallic structures are very limited [17].

In order to cope with the above two limitations, a prestressed unbonded retrofit (PUR) concept has been developed by some of the authors of the present study [17,18]. In this approach, prestressed CFRP plates are fixed to metallic girders using friction clamps (rather than adhesive bonding). Therefore, concerns related to the influence of environmental effects on bonded joints are no longer relevant. Furthermore, CFRP plates can be initially stressed up to high prestressing levels, which results in the efficient use of the high strength of this material. Therefore, the main two limiting parameters for BR systems are not relevant for the proposed PUR system, which results in an efficient and reliable technique for the strengthening of metallic bridge girders.

1.1. PUR concept

Ghafoori [17] performed the first systematic study to compare the behavior of steel members strengthened by bonded and unbonded CFRP retrofit systems. The results of extensive laboratory experiments have shown that when metallic members are retrofitted by prestressed CFRP plates, the performance of the CFRP-retrofitted metallic element is more sensitive to the pre-stress level than to the presence of the bond [19].

PUR systems are versatile and can have different configurations to cope with the geometrical complexities of metallic bridges. Furthermore, they have advantages compared with BR systems, as they can be applied to rough/corroded or obstructed/riveted surfaces and do not need any curing time. PUR systems also have a fast installation procedure, as they do not require surface preparation prior to the CFRP application. PUR systems are mainly advantageous for the strengthening of heritage structures, as the reversibility of the strengthened member (to the original unstrengthened form) is of great importance, and the retrofitted system can be removed from the original structure simply by disassembling the mechanical clamps.

Kianmofrad et al. [20] have presented four different variants of PUR systems for the strengthening of metallic beams: trapezoidal PUR (TPUR), triangular PUR (TriPUR), flat PUR (FPUR), and contact PUR (CPUR). An overview of the advantages, limitations, and performance of each system is provided in [20]. It has been found that all of the presented PUR systems result in almost similar improvements compared with the (reference) unstrengthened girders, and that any of them can be used for strengthening of the girders of bridges considering the existing room under the bridge, geometrical complexities of the elements, and ease of application [20].

Hosseini et al. [21] have developed and tested an FPUR system for strengthening metallic I-girders subjected to static and fatigue loading. The FPUR system can be used as an alternative when, owing to traffic, the space under the bridge is insufficient to install the TPUR system [20]. The details of this system are provided in the present work. Furthermore, Hosseini et al. have developed the concept of PUR systems for fatigue strengthening of tensile steel members [22,23]. More recently, some studies (e.g., [15,24–26]) on the application of shape memory alloys (SMAs) for the prestressed strengthening of steel plates have shown a promising future for this material. The SMA retrofit elements can be prestressed by thermal activation of the alloy [26]. SMAs are intelligent materials that can return to their original shape after they have been pre-strained and subjected to a characteristic temperature [25].

A trapezoidal PUR (TPUR) system for the strengthening of metallic beams was developed and tested under static [27] and fatigue loading [28]. The system has been used for the fatigue strengthening of a 120-year-old riveted railway bridge in Switzerland [29,30]. Each bridge girder was strengthened with three CFRP plates (each of them 50 mm wide and 1.4 mm thick), which were attached to the bridge girders using a pair of friction clamps. The concept of the constant life diagram (CLD) approach [31,32] was used for the determination of the CFRP prestressing level. The CLD approach is a methodology that foresees the lifetime of metals subjected to high cycle fatigue loading regimes [31]. According to the proposed fatigue design criteria [29], the CFRP plates were prestressed to nearly 35% of their ultimate strength, equivalent to approximately 950 MPa. This pre-stress level provided a total prestressing force of nearly 170 kN in the three CFRP plates applied to the bridge girders. Furthermore, a structural health monitoring (SHM) system was used to monitor the CFRP prestressing level for about one year after installation of the retrofit system. The results showed a very stable prestressing level in the CFRP plates, confirming the effectiveness and reliability of the applied retrofit system.

1.2. Structure of the study

The current study aims to present the results of the prestressed CFRP strengthening and long-term monitoring of an old metallic roadway bridge, the Diamond Creek Bridge in Melbourne, Victoria, Australia. The paper has three different sections. The first section describes the laboratory tests on a new type of PUR system, the FPUR system. The laboratory tests included pull-off tests on the developed mechanical clamping system, and static and fatigue tests on 6.4-m long steel I-beams under four-point bending conditions. After the successful development and testing of the FPUR system, the second section of this study explains the procedure for the CFRP strengthening of the Diamond Creek Bridge. Details of different aspects of the bridge strengthening, fatigue design criteria, and the most important results of short-term measurements are provided. Finally, the third part of this study focuses on the application of a wireless sensor network (WSN) system for long-term monitoring of the behavior of the bridge after strengthening. The results of laboratory tests on strain-gauge measurements of the CFRP plates inside a climate chamber with and without dummy samples are explained. Furthermore, a series of recommendations for the application of dummy samples for long-term structural monitoring is provided. Finally, preliminary results of the long-term wireless monitoring of the bridge after strengthening are discussed and interpreted.

2. Development of the FPUR system

2.1. Overall view and pull-off tests

An FPUR system was designed, manufactured, and tested at the Structural Engineering Research Laboratory of the Swiss Federal Laboratories for Materials Science and Technology (Empa). As shown in Fig. 1, the FPUR system relies on two sets of mechanical clamps, which transfer the prestressing force of the CFRP plates to the lower flange of the steel girders via friction. Each set of mechanical clamps holds two prestressed normal-modulus (NM) CFRP plates with cross-sectional dimensions of 50 × 1.4 mm (width × thickness). The strengthening procedure using the proposed FPUR system (see Fig. 1) is as follows:

(1) the non-stressed CFRP plates are anchored on one side of the beam using a so-called *fixed clamp* with the help of eight M20 high-strength (grade 12.9) bolts, which are tightened with a torque of 605 N·m, to generate a prestressing force of 223 kN per bolt.
(2) On the other side, the non-stressed CFRP plates are gripped in a so-called *movable clamp*, and the clamp set is free to move horizontally along the beam axis.
(3) Two 120-kN hollow plunger cylinders are then installed adjacent to the *movable clamp* using a cylinder housing.
(4) With the help of two prestressing M16 rods, the movable clamp is

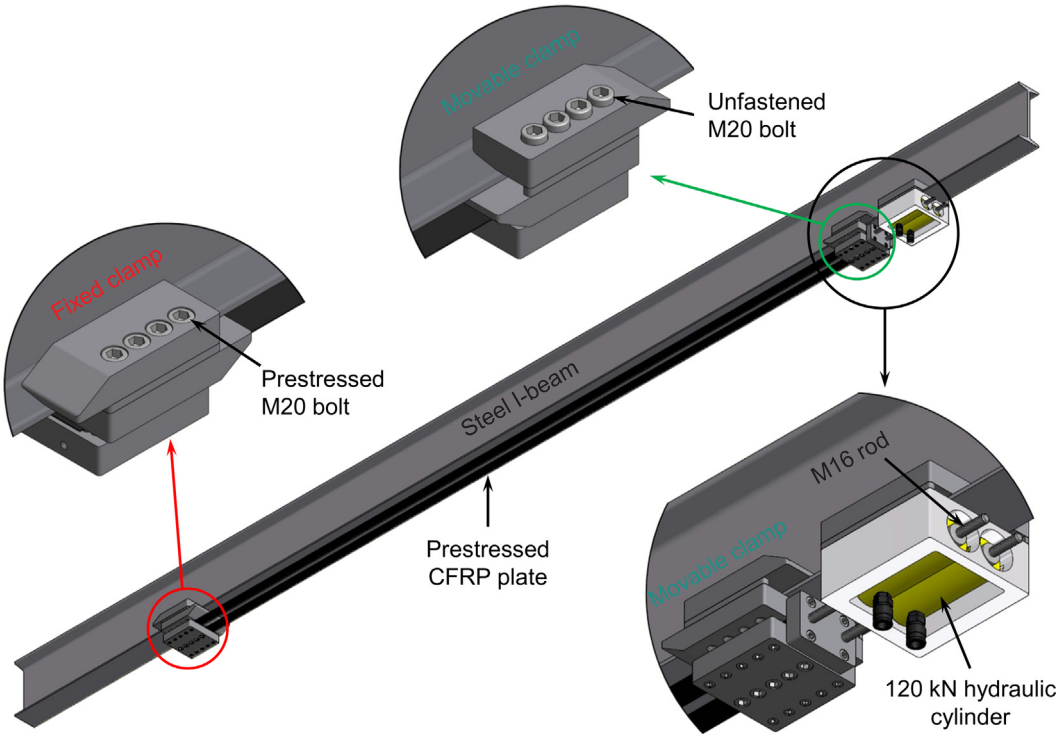

Fig. 1. Different components of the proposed FPUR system.

pulled using the hollow plunger cylinders, which are actuated using a manual hydraulic pump, and subsequently, the CFRP plates are prestressed.

(5) Upon reaching the desired pre-stress level in the CFRP plates, all the eight M20 bolts of the movable clamps are tightened.

(6) Finally, the hydraulic pressure is released and the prestressing system consisting of the two hollow plunger cylinders and the cylinder housing can be removed.

In order to optimize the geometry of the mechanical clamping system and estimate the number and diameter of the prestressed bolts (for generating the required friction force between the clamps and the tensile flange of the beam), a finite element (FE) simulation was performed using the ABAQUS FE package. More details regarding the FE simulation of the FPUR system can be found in [21]. All the required mechanical components, with the optimized geometry, were manufactured from high-strength steel M200 with a nominal yield strength of 1000 MPa.

In order to determine the ultimate capacity of the developed mechanical clamping system before slippage, a pull-off test setup was designed and a set of pull-off tests was performed on the optimized configuration of the system. Different components of the test setup are shown in Fig. 2. Figure 3 shows the strain level generated in each of the CFRP plates versus the applied load per hydraulic cylinder. It can be seen in Fig. 3 that CFRP rupture was the governing failure mode of the system, while no slippage of the clamp was observed prior to the rupture.

The NM CFRP plates of type S&P 150/2000-50/1.4 were used in this study for all the laboratory tests (in Sections 2 and 4) and for the field application reported in Section 3. The tensile strength and elastic modulus of the applied CFRP plates were 2595 MPa and 161 GPa, respectively.

2.2. Static and fatigue four-point bending tests

In order to evaluate the performance of the proposed FPUR system for the strengthening of steel I-beams, a set of static and fatigue tests was performed at the Structural Engineering Research Laboratory of Empa on 6.4-m long steel I-beams under four-point bending. Figure 4 shows different elements of the test setup and the FPUR system. The center-to-center distance of the supports was 5.3 m, while the center-to-center distance of the 250 kN hydraulic actuators was 1.8 m. First, the steel I-beam (INP 300) was loaded within the linear elastic regime up to 75 kN per cylinder (corresponding to a maximum bending stress of $0.6\sigma_y$) as the reference unstrengthened case. Afterwards, the proposed unbonded CFRP strengthening solution was applied to the steel I-beam as a flat unbonded retrofit (FUR), without any prestressing force (0% prestressing level), and the beam was reloaded up to 75 kN per cylinder. Finally, the CFRP plates were prestressed up to 20 and 40% of their tensile strength ($\sigma_{f,u}$ = 2595 MPa), and each time the beam was subjected to the four-point bending up to the same loading level.

As Fig. 5(a) and (b) show, the application of the non-prestressed unbonded CFRP plates, i.e., FUR (0%), very slightly increased the stiffness of the steel beam; however, the deflection/strain reduction in the member is not significant. It can be seen from Fig. 5(a) and (b) that application of the FPUR system with 20% or 40% prestressing level could significantly decrease the deflection and strain/stress level in the strengthened steel I-beam under service loads.

It is noted that the steel I-beams utilized in the four-point bending laboratory tests were of type S275JR with a measured elastic modulus of 203.3 GPa, and yield and ultimate strength of 328 and 465 MPa, respectively.

In addition to the four-point static tests, the performance of the FPUR system was also evaluated under four-point fatigue loading for 20 million fatigue cycles while the CFRP plates were prestressed up to 40% of their ultimate tensile capacity. The four-point fatigue test was performed under load-control conditions with a load ratio ($R = P_{min}/P_{max}$) of 0.2 and a loading frequency of 4.35 Hz. The maximum load level during the fatigue test on the INP 300 steel I-beam was equal to P_{max} = 40.2 kN per cylinder, corresponding to $0.33f_y$ in the top and bottom flanges of the unstrengthened beam.

Fig. 5c illustrates the evolution of the maximum and minimum stress levels in the FPUR system and the bottom flange of the INP300 with respect to the elapsed fatigue cycles. It can be seen from the figure

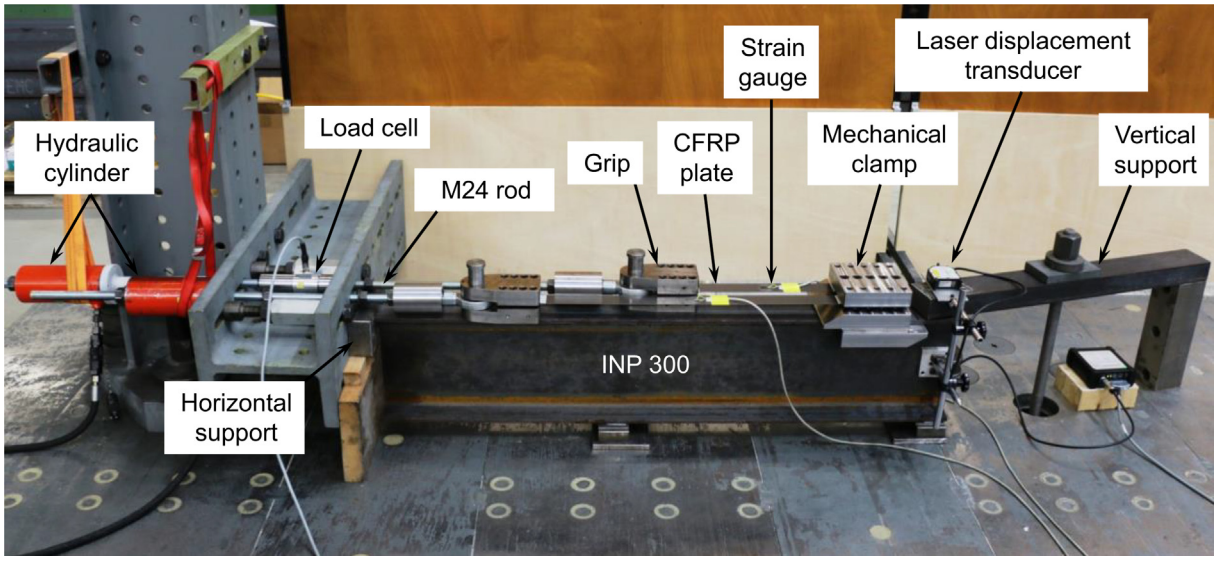

Fig. 2. Test setup for the pull-off tests on the friction mechanical clamp.

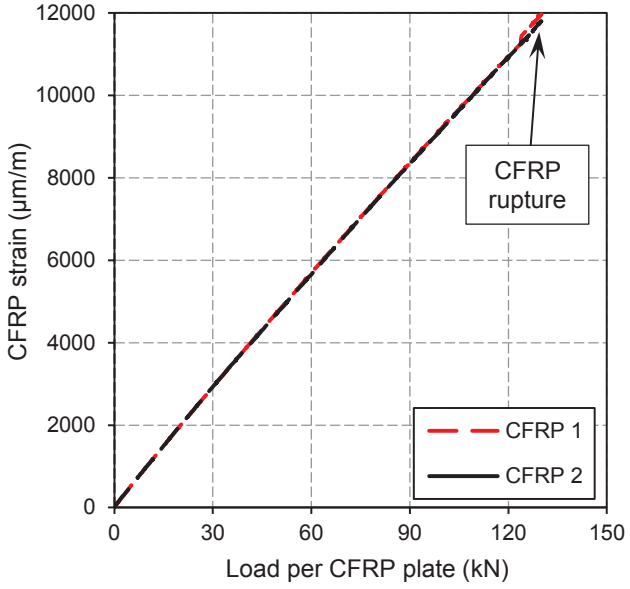

Fig. 3. CFRP strain versus load in the pull-off tests.

that during the four-point fatigue test, the maximum stress in the pre-stressed CFRP plates remained constant for the 20 million loading cycles. This proves that the proposed FPUR system experienced no slippage during the fatigue loading, as no reduction in the pre-stress level was observed. Furthermore, Fig. 5(c) shows that by applying the FPUR on the steel I-INP 300 beam, the bottom flange of the beam remains in compression for almost half of the loading range. This means that the fatigue performance of the steel I-girder can be significantly improved when strengthened using the proposed FPUR system with relatively high prestressing levels.

Note that the mechanical clamps sit at the two ends of the girder near the supports, where the bending stresses in the beam bottom flange are very low. On the other hand, the mechanical clamps were designed in a way to minimize the stress concentration. Therefore, the installation of the proposed mechanical clamps does not introduce any potential damage to the existing metallic girder [21]. This conclusion has been also proved through performing extensive laboratory fatigue tests on girders strengthened with different PUR systems, i.e., CPUR, TPUR and FPUR systems in [18,21,27,28,31]. Further information regarding the design, laboratory static and fatigue tests on the FPUR system can be found in [21]. After successful laboratory testing of the proposed system under static and fatigue loading, the system was shipped to Australia to be installed on the Diamond Creek Bridge.

3. Strengthening of Diamond Creek Bridge

The SN6091 Bridge over Diamond Creek along the Heidelberg-Kinglake Road, which was constructed in 1896, is a double-span metallic roadway bridge in Melbourne, Victoria, Australia. The bridge belongs to VicRoads, which is the road and traffic authority in the state of Victoria [33].

Fig. 6 shows the bridge elevation along with the details and dimensions of different elements of the bridges. The total length of the bridge is approximately 33 m, and it has a width of 6.4 m and a height of 2.3 m. The bridge was constructed approximately 6.4 m above the river water level. The bridge is subjected daily to the passage of passenger and heavy vehicles. It consists of two longitudinal wrought iron trusses (i.e., bottom chords) connected by several steel cross-girders, as shown in Fig. 7(a) and (b). As two different metals (i.e., steel and wrought iron) were used for the construction of this bridge, the term ‘metallic’ bridge is selected to better represent the bridge type in this study.

As shown in Fig. 6, two girders of the bridge (i.e., girders G1 and G2) were strengthened by the FPUR system. Furthermore, one girder was strengthened with a non-prestressed bonded CFRP plate. For the sake of brevity, this paper discusses only the part of the work related to the CFRP strengthening of girders G1 and G2.

Based on the available bridge documents, the steel cross-girders were of type B.S.B. 25 from the Dorman, Long & Co. Limited Company in the UK with the dimensions given in Fig. 6. Nominal Young’s modulus, yield, and ultimate strengths of 210 GPa, 250, and 320 MPa, respectively, were assumed for the mechanical properties of the steel girders. NM CFRP plates of type S&P 150/2000-50/1.4 were used for this field application, with identical material properties as those used for the laboratory tests reported in Section 2.1.

3.1. Strengthening and truck loading

After the successful accomplishment of the laboratory tests, presented in Section 2, the FPUR system was applied on two cross-girders of the Diamond Creek Bridge. For short-term on-site measurements, the bridge was subjected to a 42.5-ton semi-trailer just before and after

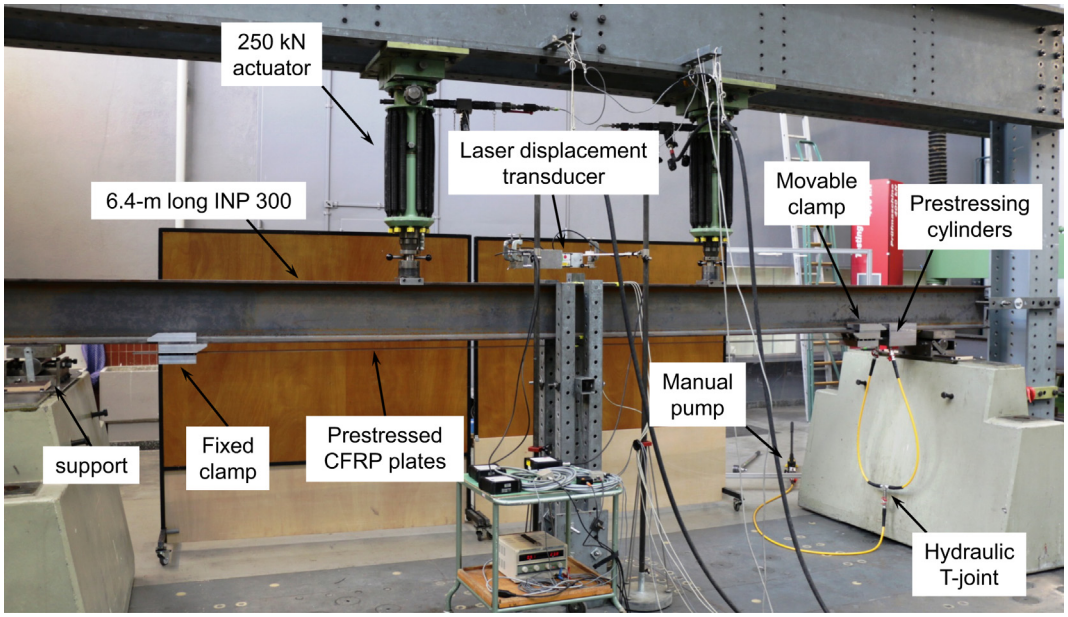

Fig. 4. Four-point bending test setup used for the laboratory static and fatigue testing of the FPUR system.

strengthening, as depicted in Fig. 7(c). The 42.5-ton semi-trailer is the heaviest vehicle allowed to cross the bridge according to the Victorian Road Authority [33]. Details of the dimensions and axle weight of the 42.5-ton semi-trailer are shown in Fig. 7(d). Based on Fig. 7(d), the first axle weighs 6 t, the second axle is a group of two individual axles and it weighs 16.5 t, and finally, the third axle is a group of three individual axles, and it weighs 20 t.

Fig. 8 depicts the strengthening procedure. It is worth mentioning that, there is no need for a proper surface treatment of the existing metallic girder for the proposed FPUR system prior to its installation, as it is the case for any bonded systems. However, prior to place the mechanical clamps on the metallic girders, the first layer of paint was removed from the area where the friction clamps sit (i.e., only a length of ≈25 cm for each clamp). Because of the following two reasons, the lead paint, which was originally used as an anti-corrosion layer, was not removed from the girders: (1) in order to prevent future corrosion of the metallic substrate where the clamps sit, (2) the lead paint is toxic and its removal process is complex, restricted, and time and cost consuming.

Different components of the FPUR system are shown in Fig. 8(a), including the cylinder housing with two hydraulic hollow plungers, manual hydraulic pump, hydraulic T-joint, hoses, movable clamp, and M16 connection rods. A wrench was used to tighten the bolts of the clamps, as shown in Fig. 8(b). Note that a similar strengthening procedure to that described in Section 2 was implemented. Finally, Tectyl™ 506 was sprayed on the mechanical clamps as an anti-corrosion coating (see Fig. 8(c)). In order to monitor the long-term behavior of the proposed FPUR system, one strain gauge was mounted onto the mid-length and mid-width of each CFRP plate using the Z70 single-component adhesive (HBM AG, Germany). Furthermore, the strain gauges were protected against humidity using the AK22 strain gauge covering material produced by HBM AG, as shown in Fig. 8(d).

Finally, the CFRP plates were prestressed and all the eight M20 bolts of the movable clamp were fastened with the allowable torque. The prestressing system consisting of the cylinder housing and two hollow plunger cylinders was then removed to obtain the final strengthened member, as shown in Fig. 9(a) and (b). The CFRP plates had the same geometrical and mechanical properties as those used in the laboratory tests and explained in Section 2.1. Figure 9(c) depicts the steel cross-girders strengthened with prestressed CFRP plates, along with the wireless sensor nodes connected to the strain gauges attached to the CFRP plates.

In order to prevent deliberate actions that may cause destruction or damage (i.e., vandalism) to the prestressed CFRP plates and WSN nodes, a protective box made out of galvanized steel was designed and attached using screws to the timber deck of the bridge, as shown in Fig. 10(a) and (b). The main goal of such protective box is to avoid any intentional or unintentional damage to the prestressed CFRP plates. In case of fire beneath the bridge, the protective box can also decelerate the process of heat transfer and damage to the prestressed CFRP plates.

In order to examine the efficiency of the proposed retrofit system, short- and long-term monitoring schemes were planned, as shown in Fig. 11. For the short-term monitoring scheme, a total of four strain gauges were applied on the four CFRP plates, while a total of six strain gauges were applied on the two cross-girders.

For the long-term monitoring, a total of four strain gauges were applied onto the four CFRP plates (one strain gauge per CFRP plate). Furthermore, the long-term monitoring scheme included one humidity and one temperature sensor.

The exact positions of the strain gauges on the CFRP plates and on the metallic cross-girders can be seen in Fig. 11. In this figure, the strain gauges used for short and long-term monitoring are shown in brown and yellow[1], respectively.

Fig. 12 shows the state of the stresses in the CFRP plates and on the top and bottom flanges of the steel girders during the prestressing process. The CFRP plates were gradually prestressed up to about 980 MPa, which is approximately equal to 38% of the CFRP ultimate strength, using a set of hydraulic actuators, as explained in Section 2. This high CFRP pre-stress level provided a total prestressing force of about 137.2 kN for the two CFRP plates, which resulted in a substantial compressive stress in the bridge girders. In Fig. 12, it can be seen that an increase in the CFRP pre-stress level results in an increase in the magnitude of the compressive stress at the beam bottom flange. After the end of the prestressing process, a compressive stress of about 30 MPa was imposed on the beam bottom flange.

The strengthening was performed on a scaffolding platform under the bridge, without closing the bridge or causing any interruption to traffic over the bridge. In Fig. 12, the sudden (small and large) jumps of the stresses are attributed to the passage of vehicles (regular daily

[1] For interpretation of color in Figs. 11, 14 and 15, readers are referred to the online version of this article.

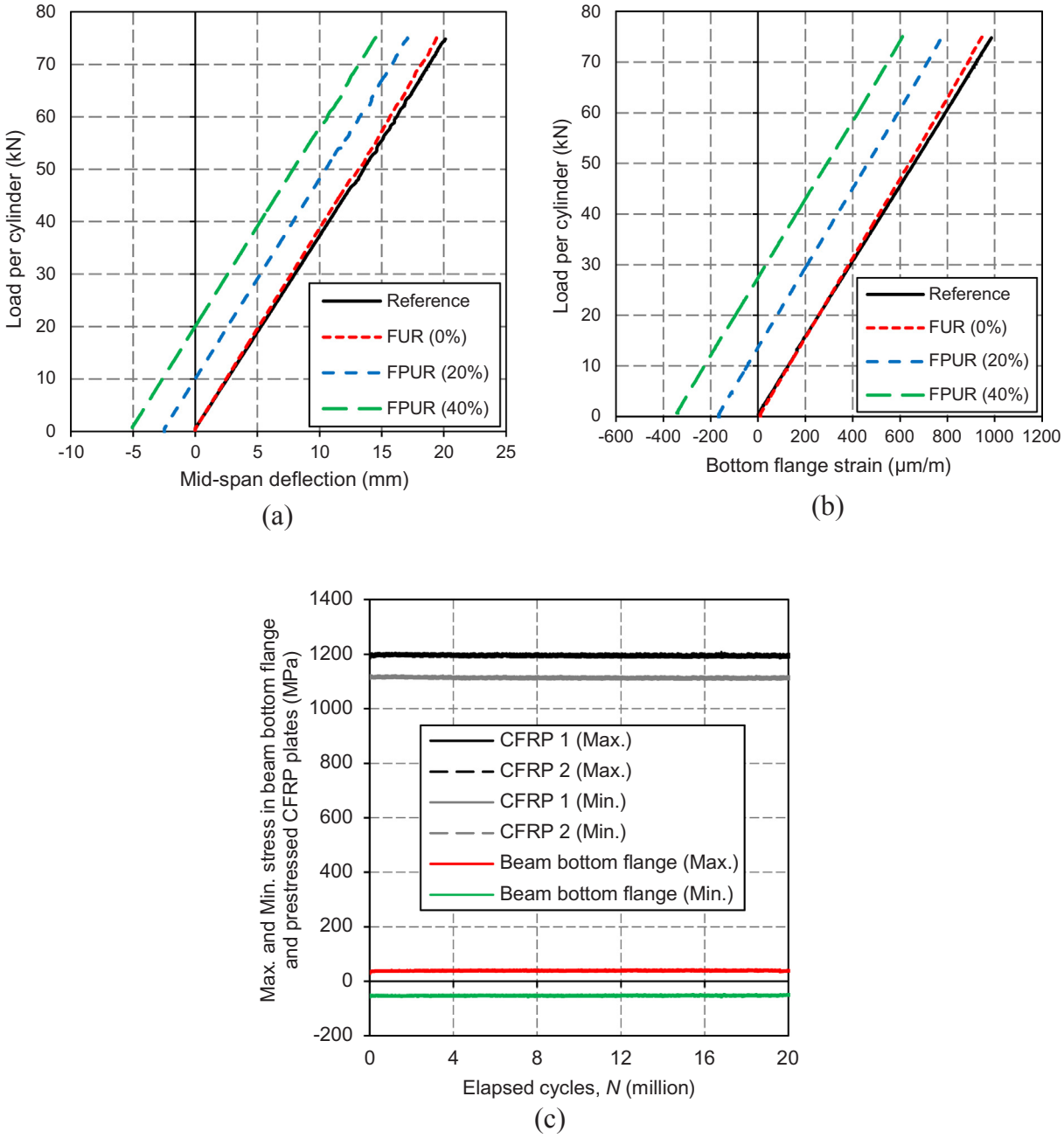

Fig. 5. Experimental results of the four-point bending tests: (a) static load-deflection response; (b) static load-strain response of the beam bottom flange; (c) evolution of the minimum and maximum stress in the beam bottom flange and prestressed CFRP plates in response to elapsed fatigue cycles.

traffic) over the bridge during the prestressing process. Furthermore, the prestressing process was performed quickly, and it took about 200 s (see Fig. 12). Truck loading tests were performed for the short-term measurements before and immediately after strengthening of the bridge girder using the 42.5-ton semi-trailer shown in Fig. 7(d).

Fig. 13(a) shows the stresses at the bottom flanges of the mid-span of girder G2 owing to the passage of the 42.5-ton semi-trailer at a slow speed, of about 5 km/h, before and after strengthening. In this figure, it can be seen that the maximum tensile stress in the beam bottom flange before strengthening was about 80 MPa, which was then reduced to about 40 MPa after strengthening with the FPUR system. This shows a reduction of about 50% (i.e., ≈ -40 MPa) of the maximum tensile stress in the bridge cross-girder. Note that 30 MPa (out of 40 MPa decrease) were due to the application of prestressing (see Fig. 12) and only 10 MPa were because of the increased stiffness of the girders after CFRP strengthening.

Furthermore, in Fig. 13(a), three stress peaks can be observed for each stress curve. The first, second, and third stress peaks are related to the first, second, and third axle group of the truck, respectively. The third stress peak, which is associated with the highest stress level in Fig. 13(a), is attributed to the last (i.e., third) axle load of the truck, which includes a group of three individual axles with a total weight of 20 t (see Fig. 7(d)).

Furthermore, Fig. 13(b) indicates that the magnitude of the compressive stress in the top flange of the cross-girder slightly decreased after strengthening. Figure 13(c) shows the stress history in the CFRP plate owing to the passage of the 42.5-ton semi-trailer. The stress in the CFRP plate increased by about 62 MPa (i.e., about 2% of the CFRP's ultimate strength) owing to the passage of the truck. Note that if the CFRP plates had not been prestressed, only a negligible portion of the

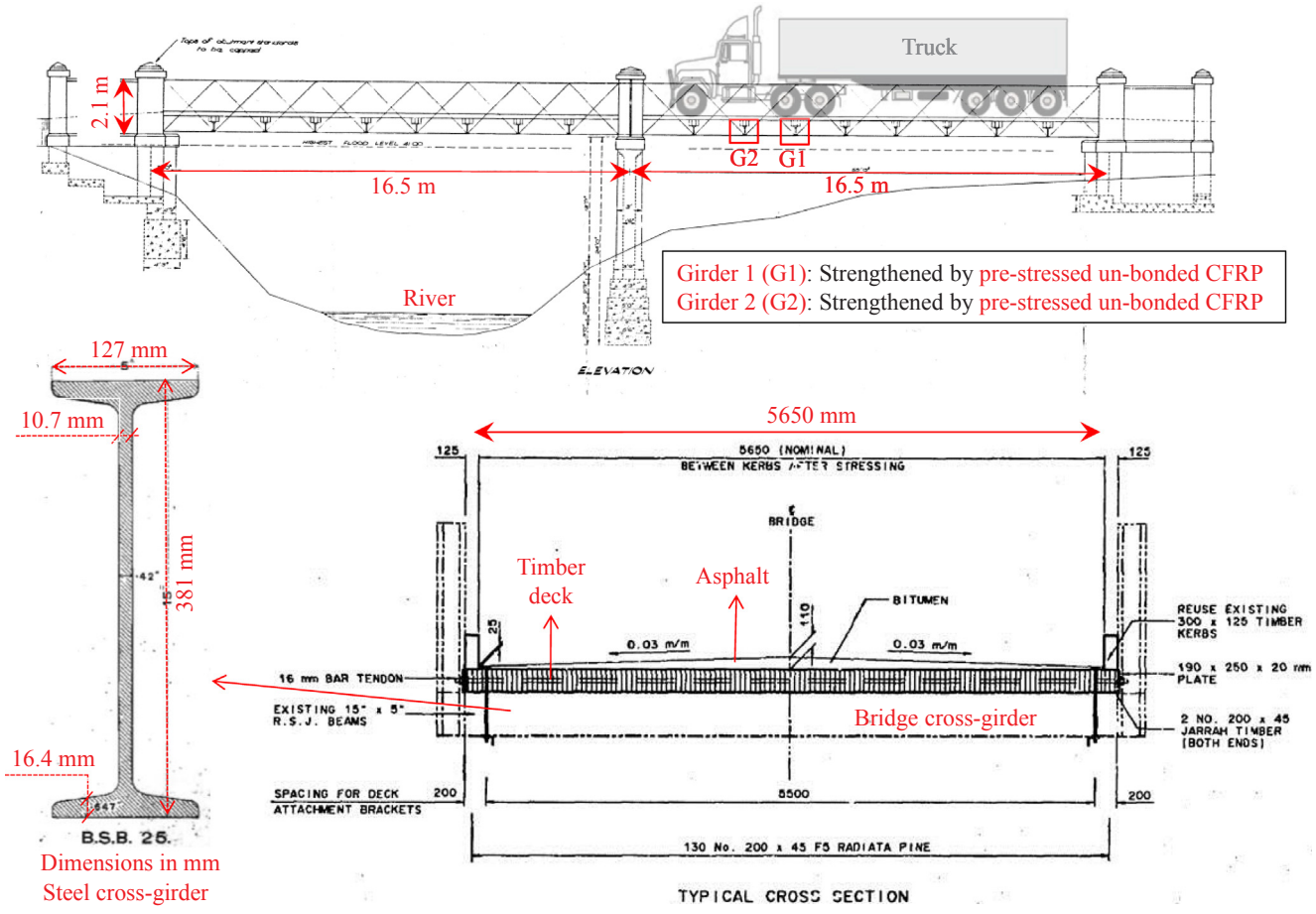

Fig. 6. Schematic view of the Diamond Creek Bridge and bridge cross-girders (figures not in the same scale).

high tensile capacity of the CFRP material would have been utilized. Nevertheless, because the CFRP plates were prestressed up to 38%, the maximum stress in the CFRP plates reached about 1042 MPa during the truck loading, which is more than 40% of the CFRP's ultimate strength. This result shows that the high tensile capacity of the CFRP materials has been effectively utilized in this strengthening work. Note that the results of prestressed strengthening and testing of the G3 girder were very similar to those for the G2 girder, and are therefore not presented here for the sake of brevity.

3.2. Fatigue strengthening criterion

It has been shown by some of the present authors in [32] that the application of prestressed CFRP can increase the fatigue life of steel girders substantially. Ghafoori and Motavalli [31] have suggested a CLD approach to estimate the required prestressing level that results in the complete prevention of fatigue crack initiation in old metallic girders. The CLD approach is often used to establish the combined effect of mean stress level, stress range, and material properties. CLDs can predict the fatigue life of materials at various stress levels. For a given minimum stress (σ_{min}) and maximum stress (σ_{max}), the stress amplitude (σ_a) and the mean stress (σ_m) are, respectively,

$$\sigma_a = \frac{\sigma_{max} - \sigma_{min}}{2} \quad (1)$$

$$\sigma_m = \frac{\sigma_{max} + \sigma_{min}}{2} \quad (2)$$

Furthermore, the stress ratio, R, is expressed as

$$R = \frac{\sigma_{min}}{\sigma_{max}} \quad (3)$$

Fig. 14 shows the concept of the CLD approach [32]. In this figure, the horizontal axis is the mean stress, σ_m, and the vertical axis is the alternating stress, σ_a. Different fatigue failure criteria along with their mathematic formulations can be also seen in this figure. The fatigue failure criteria include the Gerber, Goodman, and Johnson criteria [34]. It has been shown by Ghafoori [29] that the Goodman fatigue failure criterion can be used as a fatigue design criterion for the determination of the safe service stresses of old metallic bridge members. In Fig. 14, the area shaded with blue inside the Goodman criterion presents a "safe zone", which implies a theoretically infinite fatigue life domain. Although the Goodman fatigue failure criterion presents safe service stresses accurately, it requires the calculation of different Marin's parameters [28]. However, the Johnson fatigue failure criterion is simple and conservative. The Johnson criterion is shown in Fig. 14 in the first quadrant and is written as [29]

$$3\sigma_a + \sigma_m = S_{ut}/n \quad (4)$$

where σ_m and σ_a are the mean and alternating stresses, respectively, at the critical location of the metallic detail. Furthermore, n and S_{ut} are the safety factor and the ultimate tensile strength of the material, respectively. Note that Eq. (4) was derived from the average values of the test results. However, as the results of fatigue tests show often a great scatter, a reliability coefficient is considered in this approach to take into account the scatter of the fatigue test data (see Appendix A). The lower reliability factor, the higher safety in term of scatter of the fatigue data (based on the probabilistic analysis). On the other hand, the safety factor, n, in Eq. (4) indicates how much stronger the retrofitted metallic member is in terms of fatigue strength than it needs to be under a given load condition. More information about the concept of the reliability coefficient, the safety factor, the CLD approach and different fatigue

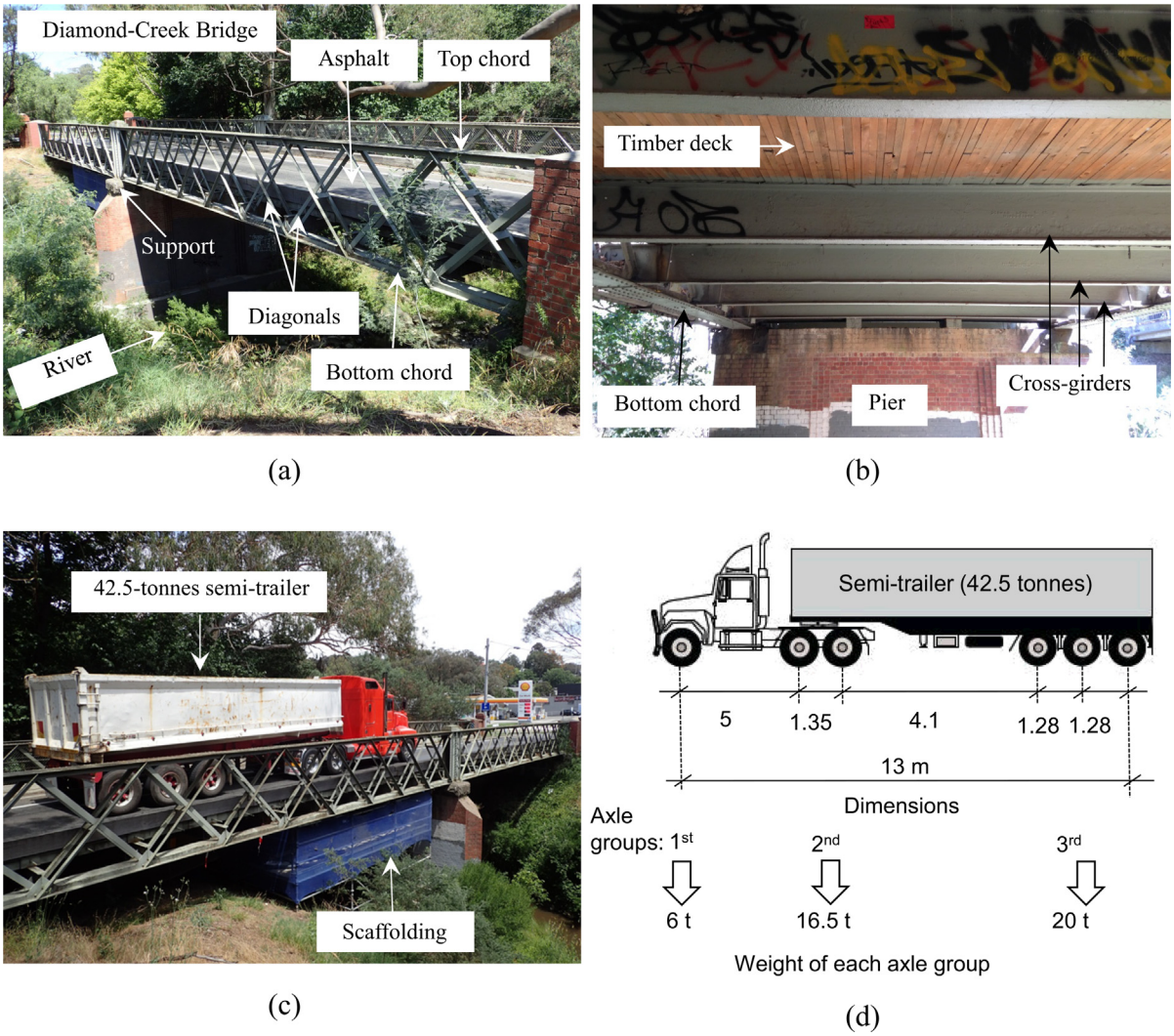

Fig. 7. (a) Diamond Creek Bridge, Melbourne, Australia, (b) flooring system of the bridge, (c) loading of the bridge using a 42.5-ton semi-trailer before and after strengthening, (d) details of the dimensions and axle weight of the truck.

failure criteria can be found in [28,29,31,32].

In this study, the Johnson criterion was used to check the fatigue performance of the cross-girders of the Diamond Creek Bridge before and after strengthening. This is because the Johnson fatigue failure criterion is simple, works with minimum prior knowledge about the existing steel members, and requires only the tensile strength of the steel, as shown in Eq. (4). While the Goodman criterion is generally more accurate for the prediction of fatigue failure, it requires much information for the calculation of different Marin's coefficients for the evaluation of the fatigue endurance limit, S_e [29]. Additional information regarding Marin's coefficients to calculate the fatigue endurance limit for the Goodman criterion can be found in Appendix A.

Note that this study aims to only use the proposed fatigue criterion, described in this section, to evaluate the fatigue performance of the girders before and after strengthening. The validity of the proposed fatigue retrofit design criterion has been extensively studied in the earlier works of the authors (e.g., [28,32]).

3.3. Fatigue strengthening parameters and results

Fig. 15 shows a CLD diagram depicting the design approach used for the fatigue strengthening of the bridge girders. Stress points A and B in Fig. 15 refer to the state of the service stresses in the beam bottom flange before and after strengthening, respectively. An initial stress level of about 12 MPa was assumed in the bottom flange owing to the deadweight of the structure. A safety factor of n = 1.04 was considered in the design [29].

The Johnson line intersects the vertical axis (i.e., alternating stress) at a stress level of $\frac{106.7}{n}$ = 102.6 MPa. Note that the value of 106.7 MPa refers to the endurance limit based on the Johnson criterion, which is one third of the steel ultimate strength [29], i.e., $\frac{320}{3}$ = 106.7 MPa.

The magnitudes of the different Marin's coefficients required to calculate the fatigue endurance limit according to the Goodman criterion are determined in Appendix B. Finally, an endurance limit of S_e = 100.8 MPa was determined (see Appendix B), which is very close to that predicted by the Johnson criterion (i.e., 106.7). This shows that although the Goodman criterion needs much information about the state of the metallic girders, it results in an almost identical fatigue assessment to that provided by the Johnson criterion [29]. More information regarding the determination of Marin's coefficients can be found in Appendices A and B.

According to Fig. 13(a), σ_{min} and σ_{max} on the bottom flange of the bridge cross-girder owing to the passage of the semi-trailer (before strengthening) were −4.5 and 82.3 MPa, respectively. By considering 12 MPa tensile stress owing to the deadweight of the structure, σ_m and σ_a were determined as 50.9 and 43.4 MPa, respectively, as depicted by point A in Fig. 15.

After strengthening with the prestressed CFRP, σ_{min} and σ_{max} owing

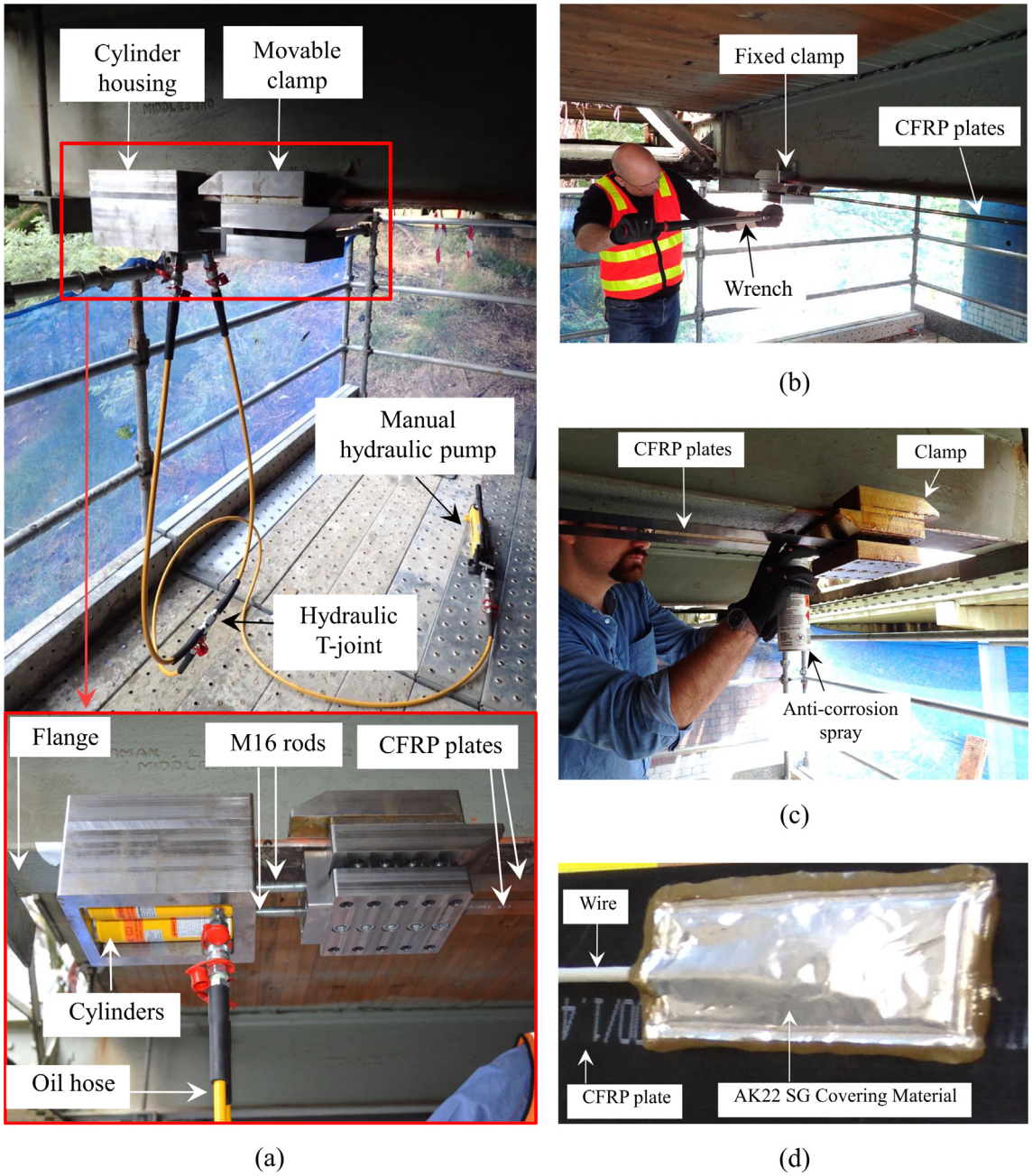

Fig. 8. Strengthening procedure: (a) assembling different components of the FPUR system, (b) tightening of the clamp bolts using a torque wrench, (c) application of anti-corrosion spray, (d) application of AK22 covering material to protect the strain gauges against humidity.

to the passage of the same semi-trailer were −35 and 42 MPa, respectively. These stresses (after considering the deadweight) result in σ_m = 15.5 MPa and σ_a = 38.5 MPa, as shown by point B in Fig. 15.

The blue arrow connecting the stress points A to B represents the effect of prestressed-CFRP strengthening within the CLD approach. In Fig. 15, it is observed that application of the FPUR system decreases the mean, σ_m, and alternating stresses, σ_a, by about −35.4 and −4.9 MPa, respectively. Note that the reduction in the mean stress, σ_m, after strengthening is seven times greater than that for the alternating stress, σ_m. The reduction in the mean stress level is attributed to CFRP prestressing, while the change in the alternating stress is a result of the increased stiffness of the girder owing to the stiffness of the CFRP material.

As Fig. 15 shows, point A, which refers to the stress state in the girder prior to strengthening, is already inside the safe region determined by the Johnson criterion. This is because the cross-girders are simple hot-rolled members without any rivets. Nevertheless, riveted built-up girders are often used in such old metallic bridges. In such cases, the rivet holes introduce stress concentrations and increase the stress levels two to three times, which then result in service stresses outside the safe zone. An example of such a case is the Münchenstein metallic railway bridge (120 years old) in Switzerland [29].

Based on Fig. 15, the stresses prior to the strengthening (i.e., point A) are inside the safe zone, and, therefore, there is no risk of crack initiation in the cross-girders. Nevertheless, the girders were still strengthened in order to enhance their flexural behavior. It is also worth mentioning that one of the main intentions of this pilot strengthening project was to demonstrate the great capability of the proposed prestressed-strengthening solution for enhancing the fatigue and flexural performance of such old fatigue-prone metallic members.

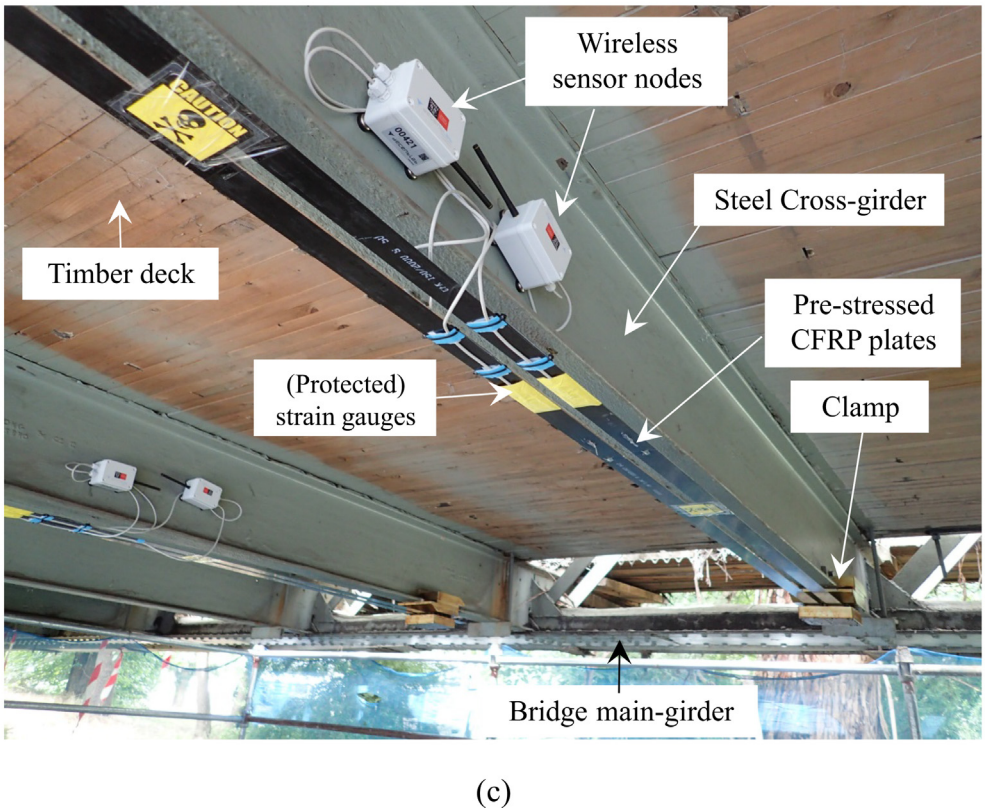

Fig. 9. (a) Bridge cross-girders after strengthening, (b) mechanical clamps and prestressed CFRP laminates, (c) different elements of the strengthening and monitoring system installed on the bridge girders. The strain gauges were protected against humidity for the long-term outdoor applications.

After strengthening through the FPUR system, the service stress in the girder bottom flange was shifted to point B. According to Fig. 15, the stress before strengthening (i.e., point A) was inside the safe fatigue region. Nevertheless, the main aim of strengthening the girders, as explained earlier, was to demonstrate the feasibility and effectiveness of using the FPUR system to decrease the service stresses in the girders. This point can be clearly observed in Fig. 15.

Based on these results, it is understood that the application of prestressed CFRP plates can substantially decrease the component of the mean stress in the steel girder, while it decreases the stress amplitude only negligibly.

4. Long-term wireless sensor monitoring system

SHM of various kinds of civil infrastructures has recently been performed using WSN technology [35]. Wireless monitoring systems have several advantages, including the simple and cable-free deployment of sensors, which minimize the cost and time of installation of monitoring projects [36]. Continuous long-term monitoring of structures provides a vast amount of data, which is difficult to sort out. Therefore, an event-based triggering WSN monitoring system was developed at the Structural Engineering Research Laboratory of Empa and used for the long-term monitoring of the Münchenstein Bridge in Switzerland in 2015 [37]. In this system, in order to reduce battery consumption, all WSN sensor nodes remain idle. A software triggering mechanism has been designed such that it activates the WSN system

Fig. 10. (a) In order to prevent any damage to the prestressed CFRP laminates owing to vandalism, a simple protective box made out of galvanized steel was installed; (b) the protective box was hanged from the timber deck (using screws).

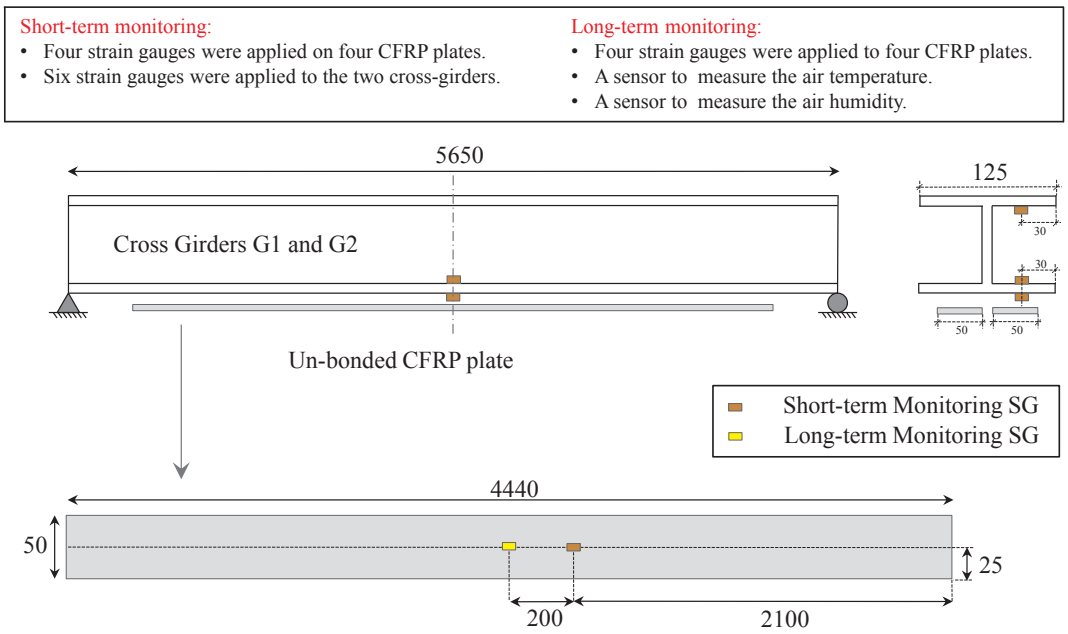

Fig. 11. Layouts of sensor placements for the short- and long-term monitoring schemes on the steel cross-girders of the Diamond Creek Bridge and the unbonded prestressed CFRP plates.

when a train/truck approaches the bridge. Consequently, the WSN nodes start to record the data with high frequency and then go to the idle mode (i.e., sleeping mode) until the next train/truck approaches the bridge. More information about the event-based WSN triggering systems can be found in [37].

In the present study, the WSN system was used for the long-term monitoring of the prestressing level in the CFRP plates after installation on the Diamond Creek Bridge. Note that as the main aim of using the WSN system was to monitor a possible change of the prestressing in the CFRP plates, there was no need to use the WSN triggering system. The sensor nodes were programmed to send the measurement data every 10 min, whether there was traffic on the bridge or not.

As shown in Fig. 11, one strain gauge was glued onto each CFRP plate and protected against humidity using AK22 covering material (see Fig. 8(d)). Figure 16 shows a scheme of the architecture of the WSN system used for the long-term monitoring of the Diamond Creek Bridge. The system includes six sensor nodes (i.e., four strain gauges, one temperature sensor, and one humidity sensor). Each sensor node includes two batteries, an electronic board, an antenna, and a terminal, as shown in Fig. 17(a). The sensor nodes are attached to the steel girders of the bridge. The housings of all the WSN nodes (i.e., the strain gauges and the temperature and humidity sensors) were equipped with four magnetic footings, which allow simple and fast mounting of the nodes, as shown in Fig. 17(b).

The sensor nodes read the data every 10 min and send them to a gateway using radio waves (see Fig. 16). The gateway is connected to an electrical power supply and can be placed within 1 km from the bridge. The gateway sends the data to a data server in Switzerland (see Fig. 16) using a 3G mobile data sim. The gateway works in a similar way to a modem, receiving the data from the sensor nodes and sending them to the server via an internet connection. The data are then backed-up in a data server and are available online and accessible to different users worldwide. Users can see online results of the measurements from the four strain gauges and the temperature and humidity sensors (see

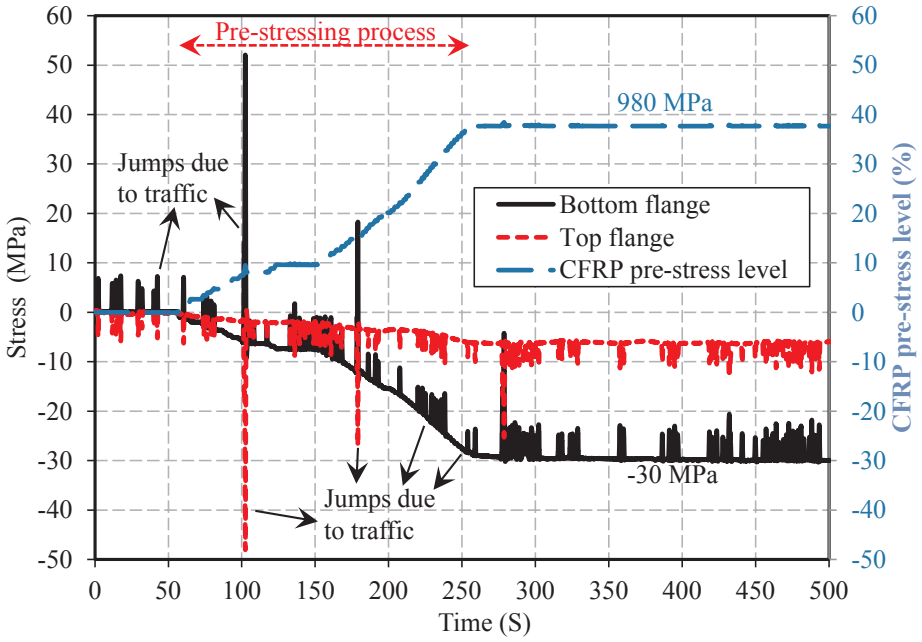

Fig. 12. Prestressing procedure: an increase in the CFRP pre-stress level results in an increase in the magnitude of the compressive stress at the beam bottom flange.

Fig. 17(c)) for at least one year using an online webpage. More discussion about the interpretation of the WSN results is provided in Section 4.3. The electronic modules of the WSN monitoring system were provided by Decentlab GmbH, Switzerland.

4.1. The use of dummy CFRP samples to compensate the temperature effect

The temperature change during the strain gauge measurements often results in an undesired influence on the strain readings. Appendix C explains the effect of temperature changes on the results of strain gauge measurements. This section explains the application of dummy CFRP samples for long-term strain measurements of CFRP-strengthened members. Note that the concept and application of the dummy samples to compensate temperature effects is not new and have been used in different fields (e.g., mechanical and civil structures) in the past. Nevertheless, the application of dummy samples for long-term monitoring of the CFRP-strengthened members is sometimes overlooked as its influence on accuracy of the final measurements is unknown and often assumed to be negligible. Therefore, this section of the study aims to quantify the error due to the lack of dummy samples when monitoring CFRP-strengthened steel members subjected to typical service temperature changes that civil structures experience.

In order to examine the influence of temperature on the readings of strain gauges applied to CFRP plates, two different tests were performed in a climate chamber at the Structural Engineering Laboratory of Empa. Figure 17(c) shows an active CFRP plate, on which two active strain gauges are attached. This figure also shows a dummy sample, which includes a small piece of passive CFRP plate and a strain gauge. Two sensor nodes are attached to the two active strain gauges on the active CFRP plate. Appendix D explains the details regarding connection of the sensor nodes to strain gauges (with half- or quarter-bridge configurations).

In order to compare the results of the strain measurements on the active CFRP plate with and without the presence of the dummy sample, all the test components including the active CFRP plate, the dummy CFRP sample, nodes 1 and 2, and the air temperature node were placed in a Zwick climate-controlled chamber, as shown in Fig. 17(d). The specimens were then subjected to a temperature range between −10 °C and 43 °C. According to the Australian Government Bureau of Meteorology [38], the extreme temperatures in Melbourne during 2017 for the coldest night (on July 2) and the hottest day (on Dec. 19) were −5.3 °C and 39.1 °C, respectively. Hence, the lower and upper temperatures selected in the Zwick climate-controlled chamber cover Melbourne's extreme temperatures.

Fig. 18(a) shows the air temperature inside the chamber versus time. Note that the active and dummy CFRP samples were not loaded in the chamber (i.e., free stress state). A heating and cooling rate of 0.2 °C/min was adopted. The measurement of the air temperature inside the chamber was performed using the wireless temperature sensor node, as shown in Fig. 17(c). Figure 18(b) shows the measurements obtained by wireless sensor nodes 1 and 2 (see Fig. 17(c)), with and without a dummy sample. It can be seen that the measurements with a dummy sample show an almost zero stress level along the active CFRP plate. However, the measurements without a dummy sample show a considerable stress change (i.e., a fake stress) ranging from about −34 MPa to 26 MPa for the temperature levels of −10 °C and 43 °C, respectively. Note that the stresses were calculated using the strains read from the strain gauges multiplied by the CFRP Young's modulus in the fiber direction.

In Fig. 18(b), the results of the test show a fake stress range of about 60 MPa (and a fake strain range of about 373 μm) for a temperature range of 53 °C (without using a dummy CFRP sample). The fake stress was determined by multiplication of the fake strain (i.e., 373 μm) and the Young's modulus of the CFRP (i.e., 161 GPa). This fake stress is undesirable and is due to the mismatch between the thermal expansion of the CFRP material and the strain gauge itself. Note that the fake stress range (i.e., 60 MPa) is significant and is of the same order as the stress level (i.e., 62 MPa) owing to the passage of the truck across the bridge (see Fig. 13(c)). This observation shows the importance of using a dummy sample when measuring the strain along CFRP reinforcement subjected to temperature changes.

In this study, in order to compensate the effect of temperature during the long-term measurement of the strain along the CFRP plates, a dummy CFRP sample was prepared for each prestressed CFRP plate. Each dummy CFRP sample, which was a piece of non-stressed CFRP plate with a passive strain gauge, was placed next to an active gauge on the prestressed CFRP plate) at the bridge girders.

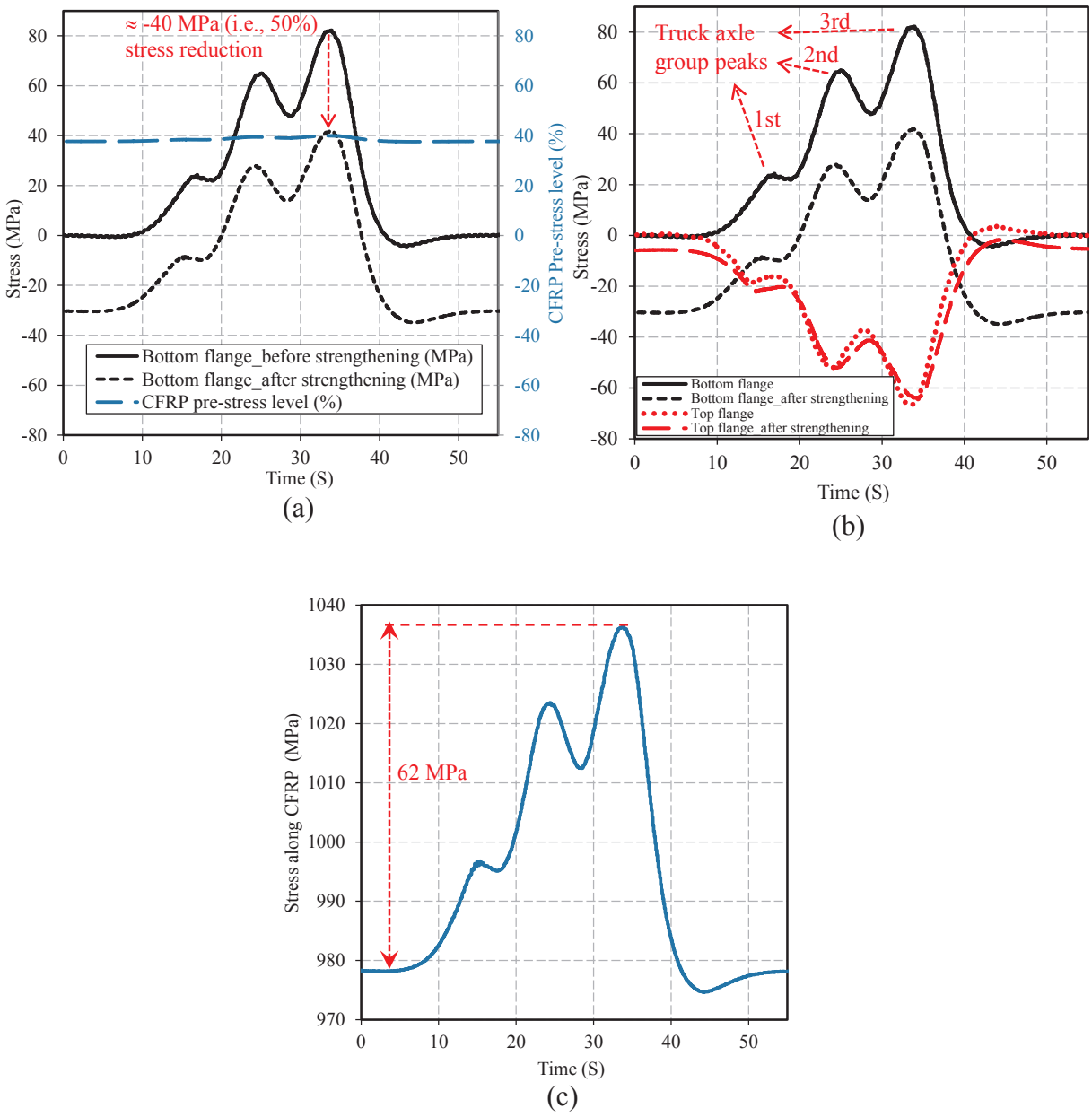

Fig. 13. Results of short-term monitoring: stress at the (a) bottom and (b) top flanges in the mid-span of steel girder G2 owing to the passage of a 42.5-ton semi-trailer before and after strengthening; (c) evolution of the tensile stress in the prestressed unbonded CFRP reinforcements owing to passage of the truck.

4.2. Long-term wireless monitoring of Diamond Creek Bridge

In order to ensure that no slippage occurs neither between the CFRP plates and clamps nor between the friction clamps and steel beam flange, one resistance strain gauge was mounted on each CFRP plate (see Fig. 11), coated with AK22 covering material for long-term protection against humidity (see Fig. 8(d)), and then connected to a sensor node together with a dummy CFRP sample (see Fig. D.1(b)).

All the strain gauges used for the WSN system were of type 1-LY46-6/700 with a k-factor of 2.03 ± 1.5% and an electric resistance of 700 Ω ± 0.30%, provided by the HBM Company, Germany. The high electric resistance of 700 Ω was selected to reduce battery consumption, and therefore, enable an increased measurement lifetime of the WSN system. All of the strain gauges and the humidity and temperature sensors were connected to the WSN nodes and sent data to the gateway, which was placed in a shop within 1 km from the bridge (see Fig. 16).

4.3. Preliminary results of long-term monitoring

Fig. 19 shows the time history of the on-site air temperature and the stress level in all the prestressed CFRP plates applied to the girders G1 and G2 of the Diamond Creek Bridge from December 1 to 14, 2017 (i.e., a duration of two weeks). Nodes 419 and 420 show the stress in the two prestressed CFRP plates attached to the girder G1, and nodes 421 and 422 refer to the two CFRP plates on the girder G2.

Fig. 19 also shows an enlarged view of the results of node 421 (i.e., one of the CFRP plates on the girder G2). This figure shows a pattern of stress fluctuations during the day and night, and some sudden jumps with small and large stress amplitudes. The stress fluctuations in this figure can be attributed to the temperature change. As the temperature increases, the CFRP pre-stress level increases, because CFRP has a negligible CTE in its fiber direction compared to that for steel. Note that steel has a CTE of 11–13 $\times 10^{-6}\,K^{-1}$ (depending on its composition); however, CFRP has a CTE of about $-0.8 \times 10^{-6}\,K^{-1}$. The mismatch

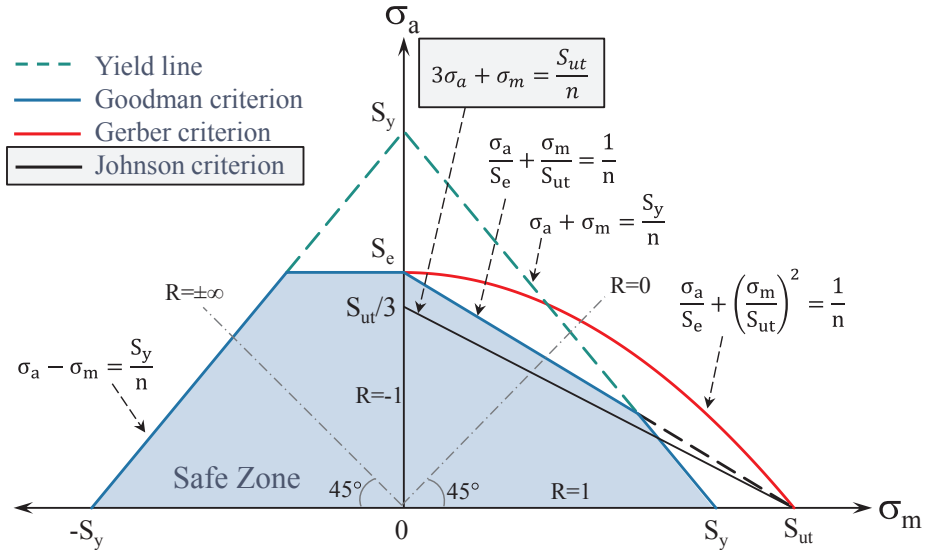

Fig. 14. CLD representing Johnson, Gerber, and Goodman fatigue failure criteria.

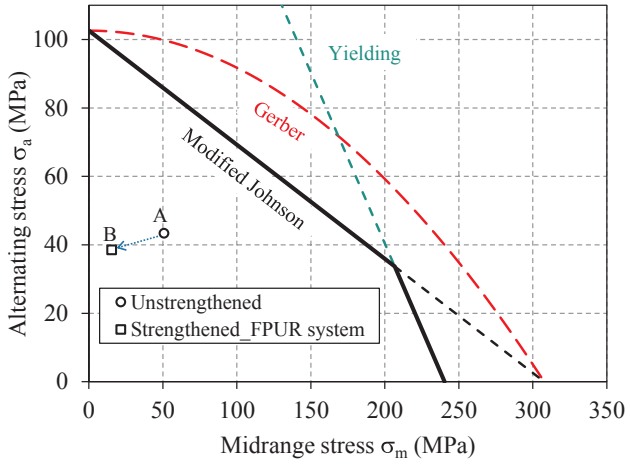

Fig. 15. CLD criteria for estimating the state of the cross-girders of the Diamond Creek Bridge before and after strengthening.

between the CTE between steel and CFRP materials is the main reason for the stress fluctuations along the CFRP plates owing to the temperature changes during nights and days. This stress change in the CFRP material owing to the temperature variation is real and is not an error in the measurements. As a separate note, the CTE for concrete is about $12 \times 10^{-6}\,K^{-1}$. Therefore, similar thermal behavior is to be expected when the CFRP material is bonded to concrete structures and subjected to temperature changes.

As shown in Fig. 19, with an increase of approximately 25 °C in air temperature, the CFRP pre-stress level increases by approximately 25 MPa, which is less than 1% of the CFRP ultimate strength. Note that this temperature effect is because of the expansion of the steel cross-girders; it is a real stress that differs from the "fake" one explained in Section 4.1.

The sudden small and large jumps observed in the CFRP pre-stress in Fig. 19 are due to the passages of small passenger vehicles and heavy trucks, respectively. As mentioned earlier, the sensor nodes were programmed to send the measurement data every 10 min, whether there was traffic on the bridge or not.

The change in the humidity did not have any influence on the CFRP pre-stress level, and therefore, it is not presented and discussed in this study. The preliminary results of the wireless monitoring system show that neither slippage nor pre-stress loss has occurred in the system to date. The WSN system will remain on the bridge for at least one year to monitor any possible pre-stress loss and study the probable effects of the temperature.

4.4. Recommendations for long-term monitoring of CFRP-strengthened metallic members

There are not many studies on long-term monitoring of CFRP-strengthened metallic members; therefore, this section aims to provide a series of recommendations (based on the experiences gained in the current study and [29]) for such applications. Note that the existing monitoring recommendations in other fields (e.g., mechanical engineering domain) cannot be readily used for this case, as the materials and working environment (e.g., typical service temperature ranges) are different.

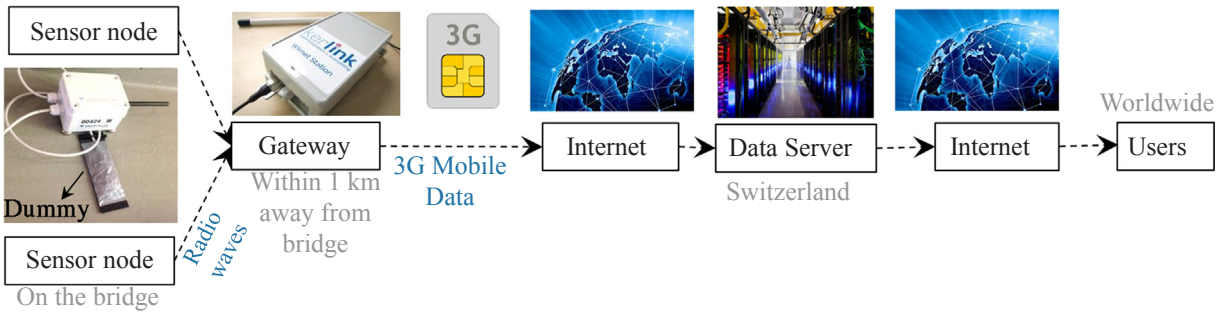

Fig. 16. Flowchart of the architecture of the WSN system used for the long-term monitoring of the Diamond Creek Bridge.

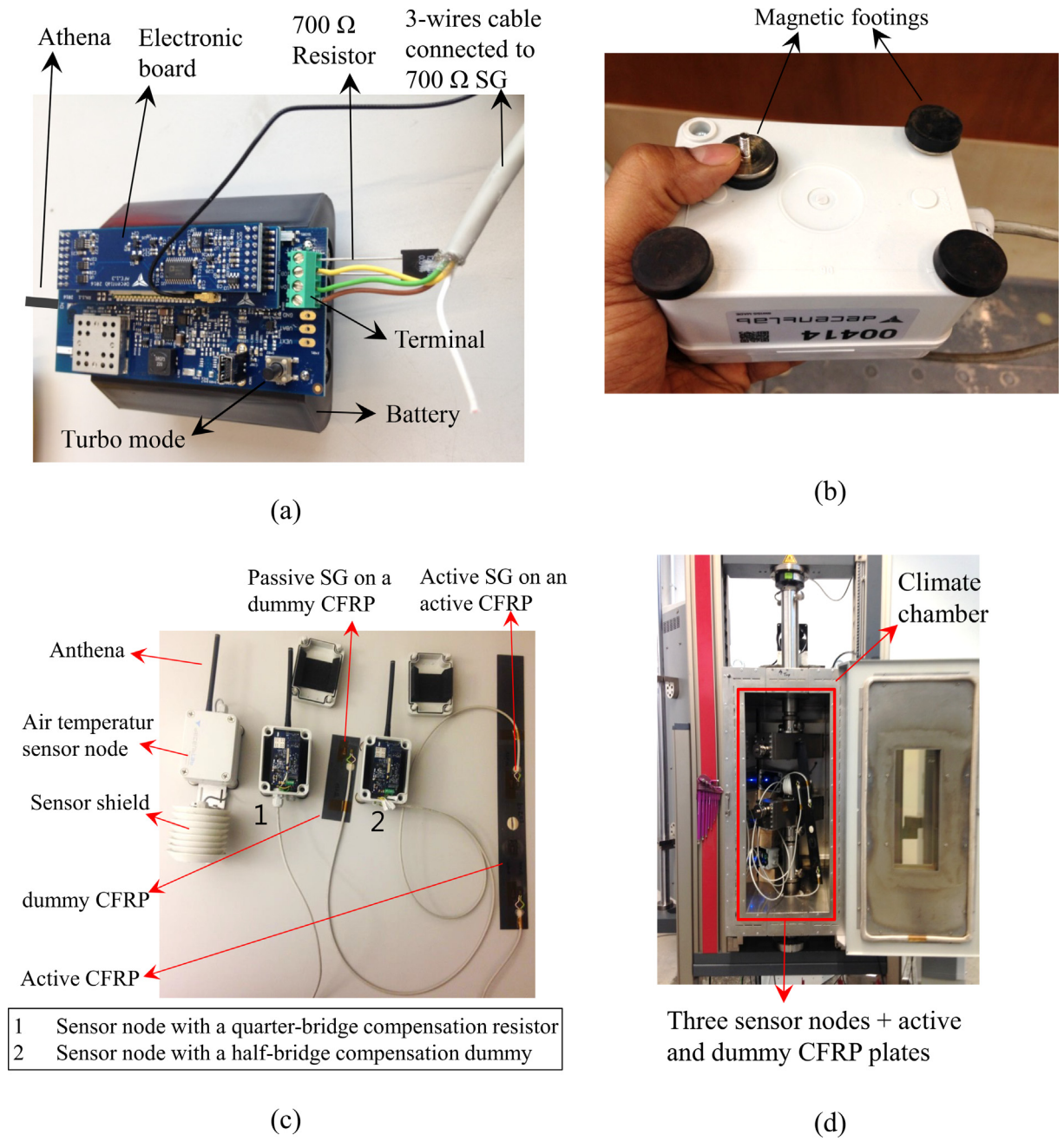

Fig. 17. (a) Different elements of a sensor node, (b) magnetic footings for a simple and fast mounting of the sensor nodes on metallic bridge girders, (c) equipment for measurements with and without a dummy sample, (d) Zwick climate-controlled chamber used for testing.

As it is explained in Appendix C, a change in temperature can substantially affect the measurements of strain gauges, resulting in undesirable fake stress interpretations. Figure 18 shows that the magnitude of such a fake stress may be as large as the stress level generated in the member owing to live loads on the bridge. Therefore, it is very important to compensate the temperature effect; otherwise, the results of long-term measurements will not be reliable, as they will include the fake strain-component owing to temperature change and the real strain caused by live loads.

As stated in Appendix C, the temperature change can affect the results of the strain gauges in two major ways: a mismatch between the CTE of the strain gauge and that of the base material, and a change in resistance of the connecting wires. Based on Section 4.1, the best way to compensate the above two components is to use a dummy sample.

The application of dummy samples is recommended for cases when the CFRP material is subjected to considerable temperature changes. These may be long-term outdoor measurements or even laboratory tests when the CFRP-strengthened member is placed inside a climate chamber. In both cases, the dummy samples should be placed under the same environmental conditions next to the active strain gauges. Although in this study the CFRP material was used for the strengthening of steel members, the same argument is valid for long-term measurement of CFRP- or SMA-strengthened concrete members.

Despite the above discussion, dummy samples are not necessary when the absolute value of the stresses in the CFRP material owing to temperature change is not relevant and only the stress change caused by loading of the structure is of interest. For example, refer to the results of the short-term measurements of the bridge in Fig. 13. Furthermore, the application of dummy samples can be neglected when the base material (see Fig. C.1 in Appendix C) has a well-known CTE; for example, when

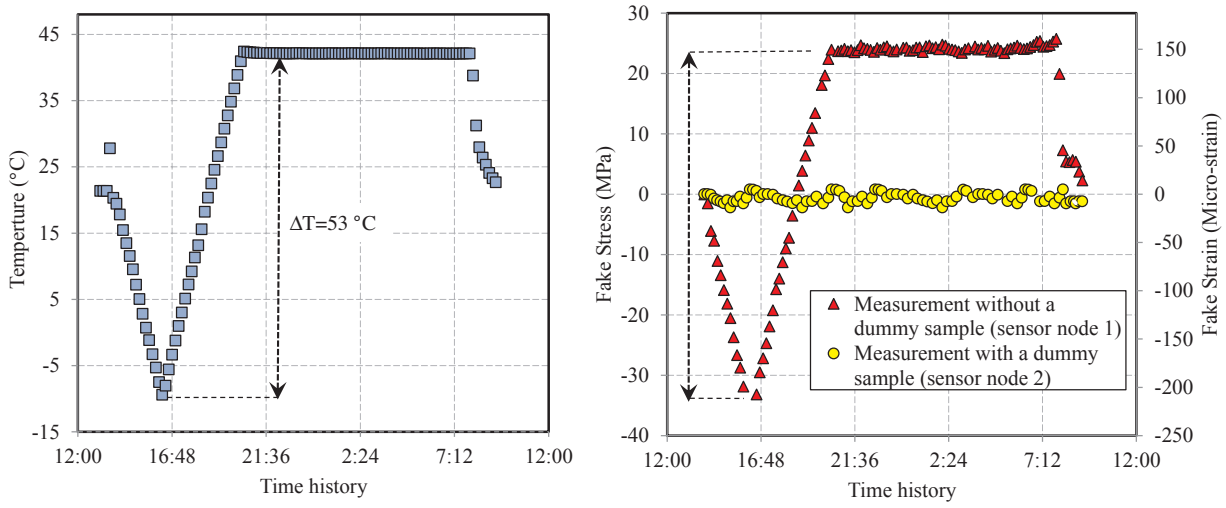

Fig. 18. (a) Temperature history inside the Zwick climate-controlled chamber, (b) results of strain measurements on the CFRP laminates with and without a dummy sample in terms of fake stress. Results show a substantial 'fake' stress in the measurements without using a dummy sample.

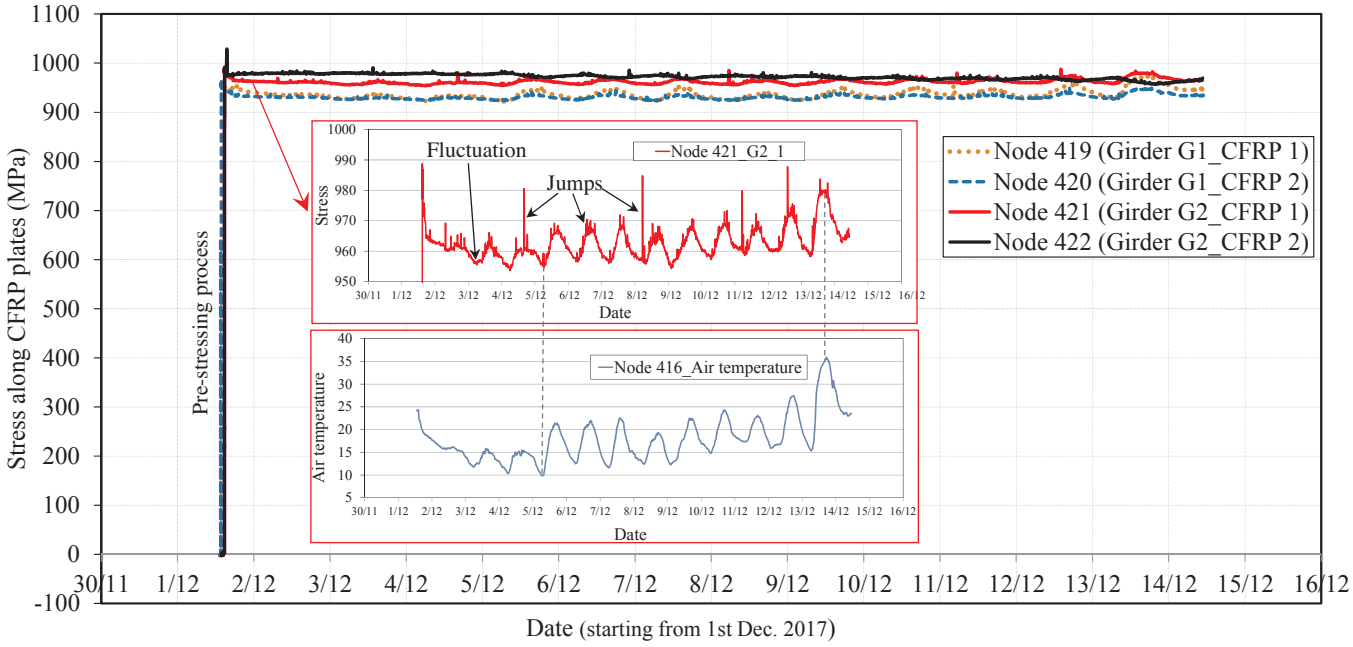

Fig. 19. Results of wireless monitoring system: time history of the pre-stress level in the four prestressed CFRP plates from December 1 to 14, 2017. The stress fluctuations are due to the daily thermal expansion and contraction of the metallic bridge, while the stress jumps are caused by traffic.

the base material is steel or concrete. However, for special cases, particularly when the base material is a CFRP (or SMA) material, it is difficult to find self-compensated strain gauges that can follow the CTE of the base material for a wide range of temperature changes. Furthermore, CFRP materials may have different CTEs, depending on whether they are plates or sheets and also on their fiber content ratio. The CTEs of certain shape memory alloys, such as Fe-SMA, can vary depending on the temperature.

Therefore, the application of dummy samples is recommended for accurate strain-gauge measurements along CFRP (and SMA) materials, particularly when the temperature changes considerably (e.g., long-term outdoor measurements or laboratory tests inside a climate chamber).

5. Summary and conclusions

This study has presented the results of prestressed CFRP strengthening and long-term monitoring of a 122-year-old metallic roadway bridge in Melbourne. The paper has three different sections. The first section explained the procedure of design and laboratory testing of the FPUR system. The second section presented the details of strengthening of the Diamond Creek Bridge. The layouts of the short- and long-term measurements were also discussed. The third section discussed the development, testing, and installation of a WSN system for the long-term structural monitoring of the retrofitted girders. Finally, the preliminary results of the long-term monitoring of the CFRP-retrofitted girders were discussed. The main conclusions for each section are summarized as follows:

5.1. First section: development and laboratory testing of the FPUR system

- The conducted pull-off tests on the developed mechanical clamping system showed that the proposed system is capable of transferring the entire tensile capacity of two 50 × 1.4 mm (width × thickness)

CFRP plates into the steel substrate. The failure mode was observed to be tensile rupture of the CFRP plate, while no slippage occurred before the failure, indicating the robustness and high performance of the developed mechanical clamping system.

- A series of static tests was performed on a 6.4-m long steel I-beam strengthened by the FPUR system with different prestressing levels of 0%, 20%, and 40% of the CFRP ultimate tensile strength. The experimental results showed that the application of the FPUR system with relatively high prestressing levels could substantially decrease the tensile stresses in the beam bottom flange under external loading, compared to the reference unstrengthened beam.
- A four-point fatigue test was performed on a steel I-beam strengthened by the proposed FPUR system with a prestressing level of 40% (≈1100 MPa pre-stress in the CFRP plates). The test results showed a high reliability for the proposed FPUR system, as the pre-stress level in the CFRP plates remained constant over 20 million load cycles (i.e., no pre-stress loss was observed).

5.2. Second section: strengthening and truck loading of the Diamond Creek bridge

- For the first time in Australia, a bridge was strengthened with pre-stressed fiber-reinforced polymer composites. Two bridge girders were retrofitted with the FPUR system. Each girder was strengthened with two CFRP plates prestressed up to about 980 MPa (≈38% of the CFRP ultimate strength). In order to prevent vandalism and to delay the damage process owing to potential fire scenarios, a simple protective box made out of galvanized steel was designed to cover the prestressed CFRP plates.
- The short-term measurements results of the truck loading using a 42.5-ton semi-trailer showed that the maximum tensile stress in the beam bottom flange was reduced from 80 MPa before strengthening to 40 MPa after strengthening. This shows a reduction of about 50% (i.e., ≈ −40 MPa) of the tensile stress in the bridge cross-girders, of which −10 MPa was due to the CFRP stiffness and −30 MPa was because of the CFRP prestressing.
- The stress in the CFRP plates increased by about 62 MPa (i.e., 2% of the CFRP's ultimate strength) owing to the passage of the truck. Therefore, it can be concluded that only a very negligible portion of the high tensile capacity of the CFRP material would have been utilized if the CFRP had not been prestressed (up to 38%).
- An endurance limit of Se = 106.7 MPa was determined for the bridge cross-girders according to the Johnson fatigue failure criterion, which is very close to that predicted by the Goodman criterion (i.e., 100.8 MPa). Johnson criterion does not require many parameters to be estimated and therefore is recommended, as an easy approach, for fatigue strengthening of old metallic bridges.
- Application of the FPUR system decreased the mean, σ_m, and alternating stresses, σ_a, by about −35.4 and −4.9 MPa, respectively. This shows that the reduction in the mean stress, σ_m, after strengthening is seven times greater than that for the alternating stress, σ_m. Note that the reduction in the mean stress level is attributed to CFRP prestressing, while the change in the alternating stress is a result of an increased stiffness of the bridge girder owing to the stiffness of the CFRP reinforcement. The latter suggests that the applied prestressed CFRP plates significantly decreased the component of mean stress in the bridge girder, while it could also decrease the stress amplitude to some extent.

5.3. Third section: long-term monitoring of the bridge

- The error due to the lack of use of dummy samples when monitoring CFRP-strengthened steel members subjected to typical temperature changes that civil structures experience was quantified. The results of the laboratory tests on the CFRP plates instrumented by strain gauges showed an undesired fake stress of about 60 MPa for a temperature change of 53 °C in the climate chamber. This considerable fake stress component is undesirable and is of the same order as the stress level in the CFRP plates during truck loading (i.e., 62 MPa).
- As it is difficult to find self-compensated strain gauges that have identical CTEs to those of the CFRP materials for a wide temperature range, the application of dummy samples is recommended for tests when CFRP materials are subjected to considerable temperature changes. These may be long-term outdoor measurements or laboratory tests when CFRP materials are placed inside a climate chamber.
- Preliminary results of the wireless monitoring system showed that no slip or pre-stress loss occurred in the FPUR system. The results of the WSN showed that with an approximately 25 °C increase in air temperature, the CFRP pre-stress increased by approximately 25 MPa (i.e., less than 1% of the CFRP ultimate strength).

Acknowledgements

The authors gratefully acknowledge the financial support provided by the Australian Research Council (ARC) Linkage Grant (LP140100543), the Swiss National Science Foundation (SNSF Project No. 200021-153609) and the S&P Clever Reinforcement Company AG in Switzerland.

Thanks are also due to Yew-Chin Koay and Hai Luong from VicRoads (Roads Corporation of Victoria, Melbourne), Marko Horvat, Jon-Paul Marrow, Cole Harvey and Jim Barraza from Aeramix Company, Martin Hüppi from the S&P AG, Sanjeet Chandra and Alaa Al-Mosawe from Swinburne University of Technology and Herb Kuhn from Simpson Strong-Tie, Melbourne, for their exceptional help and cooperation during the installation of the system on the bridge. The authors would also like to thank Slavko Tudor, Robert Widmann, Dimitri Ott and Hossein Heydarinouri from the Structural Engineering Research Laboratory of Empa for their support and help in laboratory testing and shipment of the retrofit system.

Appendix A. Marin's coefficients for Goodman fatigue failure criterion

The Goodman criterion suggests a linear line between S_{ut} and the fatigue endurance limit, S_e, as shown in Fig. 14. The fatigue endurance limit according to the results of lengthy fatigue tests [34] is expressed as

$$S'_e = 0.5\,S_{ut} \text{ for steels with } S_{ut} \leqslant 1400\,\text{MPa} \tag{A.1}$$

The Marin equation, obtained through statistical analysis, is expressed by [32]

$$S_e = k_a k_b k_c k_d k_e S'_e, \tag{A.2}$$

where k_a, k_b, k_c, k_d, and k_e are the coefficients for surface condition, size, load, temperature, and reliability, respectively. Note that S_e is the endurance limit at the critical location of the steel member for the geometry and condition of use. The procedures to determine different Marin's coefficients are summarized in the following sub-sections.

A.1. Surface condition coefficient

The tests to determine the Marin's coefficients are performed on rotating-beam specimens. The specimens have a highly polished surface. The surface coefficient is a function of the quality of the surface finish of the actual part and its tensile strength, and it is written as [39]

$$k_a = aS_{ut}^b \tag{A.3}$$

Table A.1 provides an approximation of the a and b coefficients.

Table A.1
Factors for various surface finishes [39].

Surface Finish	Exponent b	Factor a S_{ut}, MPa
Hot-rolled	−0.718	57.7
Machined/Cold-drawn	−0.265	4.51
Ground	−0.085	1.58
As-forged	−0.995	272

A.2. Size coefficient

Curve fitting of experimental results is used to determine the size coefficient for round rotating bars [40]

$$k_b = \begin{cases} 1.24d^{-0.107}, & 2.79 \le d \le 51 \ \text{mm} \\ 1.51d^{-0.157}. & 51 < d \le 254 \ \text{mm} \end{cases} \tag{A.4}$$

Eq. (A.4) is obtained for rotating-bar samples; however, for non-tubular structural members, the method of effective dimension can be used. In this method, the effective dimension, d_e, can be determined by equating the stressed area at 95% ($A_{0.95s}$) of the maximum stress to the identical cross-section area in the rotating-beam specimens [41]. The effective dimension for an I-beam section is $d_e = 0.808\sqrt{a \cdot b}$ [34]. The effective dimension can be then used in Eq. (A.4) to determine the size coefficient. For axial loading, the size coefficient is $k_b = 1$.

A.3. Load coefficient

The endurance limit is calculated through experimental analysis, and it depends on whether the experiments are conducted with rotating bending, axial, or torsion loading. The results for steel and wrought iron can be expressed by [34]:

$$k_c = \begin{cases} 1, & \text{bending} \\ 0.85, & \text{axial} \\ 0.59, & \text{torsion} \end{cases} \tag{A.5}$$

Note that $k_c = 0.9$ can be assumed for axial and torsional loading of cast iron members.

A.4. Temperature coefficient

Provided that the temperature is substantially lower or higher than the standard room temperature, brittle or yielding failure modes, respectively, also need to be investigated [34]. Eq. (A.6) provides a fourth order polynomial that can be used to calculate the temperature coefficient. This polynomial is obtained by curve fitting to the test results at various temperatures [42].

$$k_d = 0.9877 + 0.6507(10^{-3})T_c - 0.3414(10^{-5})T_c^2 + 0.5621(10^{-8})T_c^3 - 6.246(10^{-12})T_c^4 \tag{A.6}$$

Note that T_c is the temperature in degrees Celsius.

A.5. Reliability coefficient

As the above coefficients are determined by statistical analysis with considerable scatter in the results, Eq. (A.7) suggests a standard deviation for endurance limits [43]:

$$k_e = 1 - 0.08 \ z_a \tag{A.7}$$

Table A.2
Reliability coefficients according to a probabilistic analysis with a Gaussian distribution [43].

Reliability	z_a	k_e
50%	0	1.000
90%	1.288	0.897
95%	1.645	0.868
99%	2.326	0.814
99.9%	3.091	0.753
99.99%	3.719	0.702

Table A.2 presents different values for z_a, determined by a probabilistic analysis with a Gaussian distribution assumption and the corresponding reliability coefficients.

Appendix B. Determination of modified fatigue endurance limit

The values of different Marin's factors are determined in this appendix for the cross-girders of the Diamond Creek Bridge. Based on Eq. (A.3), the surface modification factor was calculated with a hot-rolled finish assumption to be $k_a = 0.92$. The outer plate of the lower flange was assumed to be subjected to a pure axial stress. Therefore, based on Eq. (A.4), the size factor for axial loading was found to be $k_b = 1$. The load factor for axial loading based on Eq. (A.5) was determined to be $k_c = 0.85$.

According to the information published by the Australian Government Bureau of Meteorology [38], a conservative temperature of $T_c = -10\,^{\circ}C$ at the location of the Diamond Creek Bridge in Melbourne, Victoria, Australia was assumed, resulting in a temperature coefficient of $k_d = 0.98$ (see Eq. (A.6)). Furthermore, according to Eq. (A.7), a reliability factor of 99% (i.e., $z_a = 2.326$) was considered, which resulted in $k_e = 0.814$.

Finally, based on Eq. (A.1), the fatigue endurance limit was determined to be $S'_e = 160\,MPa$. The modified fatigue endurance limit was then obtained from Eq. (A.2) as

$$S_e = 0.92 \times 1 \times 0.85 \times 0.988 \times 0.814 \times S'_e = 100.8\,MPa \tag{B.1}$$

The modified fatigue endurance limit after application of different Marin's factors was determined to be 100.8 MPa, which is very close to that obtained in Section 3.3 for the Johnson criterion (i.e., 106 MPa). Therefore, application of the Johnson criterion, which is much easier than the Goodman criterion, is recommended for the design of the fatigue strengthening of bridge members.

Appendix C. Effect of temperature changes on the results of strain-gauge measurements

Several parameters can affect the results of strain measurements when the temperature changes [44]. The most two important are (1) thermal expansion of the base material and (2) resistance of the strain-gauge gride and cables (see Fig. C.1). The material being measured by a strain gauge expands when the temperature rises. One way to compensate the mismatch between the thermal expansion of the base material and the strain gauge is to use self-compensated strain gauges. Self-compensated strain gauges must have very similar thermal expansion behavior to that of the base material, and hence, both the base material and the strain gauge expand/contract similarly owing to any temperature change. Furthermore, the resistance of the cables, shown in Fig. C.1, is added to the resistance of the strain gauges. In this way, any change in the temperature results in variation of the resistance of the circuit, and therefore, it affects the readings of the strain gauges. One way to compensate the effect of the temperature on the resistance of cables is to use multi-wire circuit techniques [44].

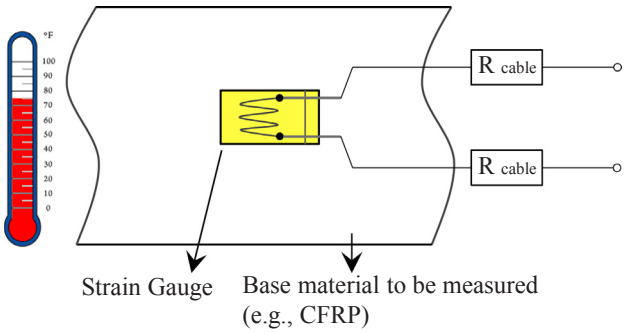

Fig. C.1. Mismatch between the CTE of the base material and the strain gauge and resistance of the cables affect the readings of strain gauges (under temperature changes).

The above two techniques can be used when the thermal behavior of the base material is well known (e.g., steel, concrete, etc.). As unidirectional CFRP materials are anisotropic composites, which are made by a pultrusion process, their exact thermal expansion behavior is directionally dependent and depends on the volume ratio of the carbon fibers in any specific direction. The coefficient of thermal expansion (CTE) for CFRP materials has often been reported as a negligible negative value of about -0.8×10^{-6}/K [45,46] in the fiber direction at room temperature, which makes it difficult to find a compatible self-compensating strain gauge for the CFRP.

In this study, strain gauges of type 1-LY46-6/700 with a gauge factor of 2.03 ± 1.5% and a resistance of 700 Ω ± 0.3%, provided by the HBM Company, Germany, were used. Although the strain gauges were ordered for measurements of strains on CFRP material, according to the HBM product data sheet, the temperature-compensation behavior of the strain gauges is set for quartz. This is possibly because, in practice, it is difficult to produce self-compensated strain gauges that can follow the exact thermal expansion behavior of CFRP with a zero or negative CTE. According to the HBM product data sheet for the received strain gauges, the quartz material has a small but still positive CTE of about 0.5×10^{-6}/K. The mismatch between the CTE of CFRP and quartz materials may create thermal stresses in the strain gauges bonded to CFRP plates. In reality, such a stress does not exist in the CFRP, but the strain gauge shows a "fake" strain value. This phenomenon is further investigated in Section 4.1.

Appendix D. Connections of the sensor nodes to the strain-gauges

The sensor node 1 (see Fig. 17(c)) was configured for a Wheatstone bridge circuit with a quarter-bridge 3-wire configuration, as shown in Fig. D.1(a). In this configuration, the effect of temperature change on the resistance of the cables is compensated through the application of multi-wire cables and a 700-Ω resistor. Note that this configuration does not compensate the effect of the thermal expansion of the CFRP material.

Sensor node 2 (see Fig. 17(c)) was configured for a Wheatstone bridge circuit with half-bridge dummy configuration, as shown in Fig. D.1(b). In

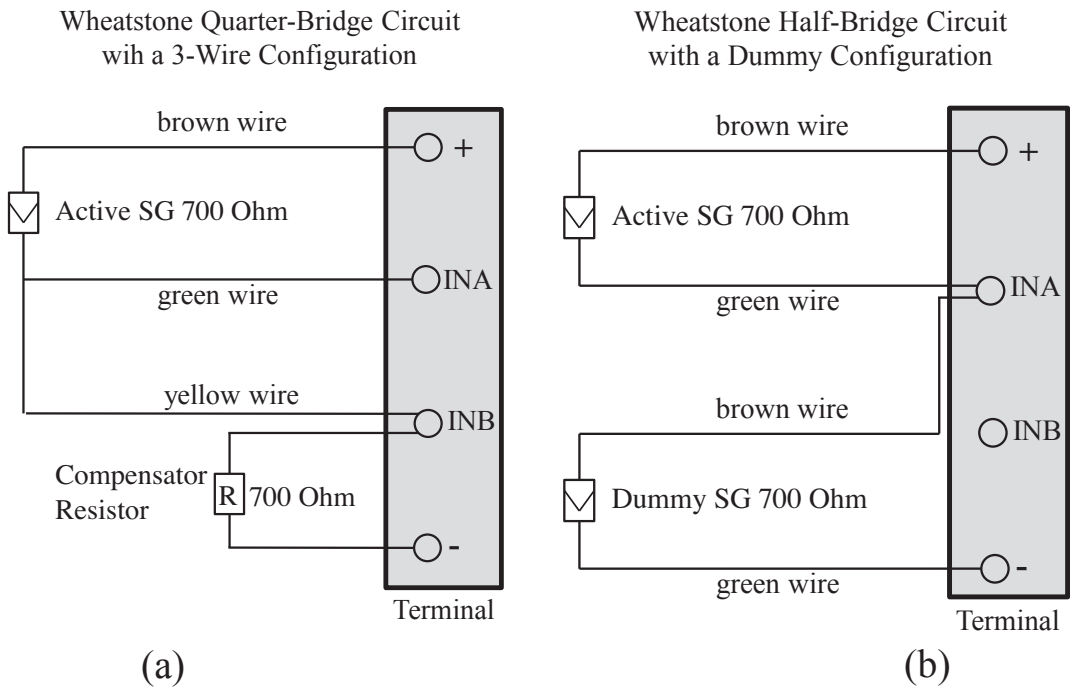

Fig. D.1. Scheme of the Wheatstone bridge circuit with (a) a quarter-bridge 3-wire configuration, (b) half-bridge dummy configuration.

this configuration, in addition to the compensation of the resistance of the cables by using multi-wire cables, the effect of the thermal expansion of the CFRP material is also compensated by using a dummy sample. The dummy CFRP plate was connected to node 2 (see Fig. 17(c)) according to the half-bridge Wheatstone-circuit configuration shown in Fig. D.1(b). Note that the length of the cables for all connections was identical and equal to 1 m. The latter configuration, shown in Fig. D.1(b), compensates both the effect of thermal expansion of the CFRP material and the resistance of the cables.

Appendix E. Supplementary material

Supplementary data to this article can be found online at https://doi.org/10.1016/j.engstruct.2018.09.042.

References

[1] Bien J, Elfgren L, Olofsson J. Sustainable bridges, assessment for future traffic demands and longer lives. Wroclaw: Dolnoslaskie Wydawnictwo Edukacyjne; 2007.
[2] Report Card for American Infrastructure, produced by American Society of Civil Engineers, transportation Bridges, 2009 Grade C.
[3] IEAust. Report card on the Nation's infrastructure. Australia: The Institution of Engineers; 1999.
[4] Yamada K, Ojio T, Inden T. Bridge monitoring and weigh-in-motion systems in Japan. In: Post-IABSE workshop on structural monitoring of bridges. Melbourne, Australia: Monash University; 2002.
[5] Zhao XL. FRP-strengthened metallic structures. Boca Raton, FL: Taylor and Francis; 2013.
[6] Al-Emrani M, Kliger R. Analysis of interfacial shear stresses in beams strengthened with bonded prestressed laminates. Compos - Part B 2006;37(4–5):265–72.
[7] Ghafoori E, Motavalli M. Flexural and interfacial behavior of metallic beams strengthened by prestressed bonded plates. Compos Struct 2013;101:22–34.
[8] Aljabar NJ, Zhao XL, Al-Mahaidi R, Ghafoori E, Motavalli M, Koay YC. Experimental investigation on the CFRP strengthening efficiency of steel plates with inclined cracks under fatigue loading. Eng Struct 2018;172:877–90.
[9] Ghafoori E, Schumacher A, Motavalli M. Fatigue behavior of notched steel beams reinforced with bonded CFRP plates: determination of prestressing level for crack arrest. Eng Struct 2012;45:270–83.
[10] Lepretre E, Chataigner S, Dieng L, Gaillet L. Fatigue strengthening of cracked steel plates with CFRP laminates in the case of old steel material. Constr Build Mater 2018;174:421–32.
[11] Colombi P, Bassetti A, Nussbaumer A. Delamination effects on cracked steel members reinforced by prestressed composite patch. Theor Appl Fract Mech 2003;39(1):61–71.
[12] Colombi P, Fava G, Poggi C, Sonzogni L. Fatigue reinforcement of steel elements by CFRP materials: experimental evidence, analytical model and numerical simulation. Proc Eng. 2014.
[13] Colombi P, Fava G, Sonzogni L. Fatigue crack growth in CFRP-strengthened steel plates. Compos Part B: Eng 2015;72:87–96.
[14] El-Tahan M, Dawood M. Fatigue behavior of a thermally-activated NiTiNb SMA-FRP patch. Smart Mater Struct 2015;25(1).
[15] El-Tahan M, Dawood M. Bond behavior of NiTiNb SMA wires embedded in CFRP composites. Polym Compos 2017. https://doi.org/10.1002/pc.24408.
[16] Schnerch D, Dawood M, Rizkalla S, Sumner E, Stanford K. Bond behavior of CFRP strengthened steel structures. Adv Struct Eng 2006;9(6):805–17.
[17] Ghafoori E. Fatigue strengthening of metallic members using un-bonded and bonded CFRP laminates PhD Thesis ETH-Zurich; 2015https://doi.org/10.3929/ethz-a-010453130.
[18] Ghafoori E, Motavalli M, Botsis J, Herwig A, Galli M. Fatigue strengthening of damaged metallic beams using prestressed unbonded and bonded CFRP plates. Int J Fatigue 2012;44:303–15.
[19] Ghafoori E, Motavalli M. Lateral-torsional buckling of steel I-beams retrofitted by bonded and un-bonded CFRP laminates with different pre-stress levels: experimental and numerical study. Constr Build Mater 2015;76:194–206.
[20] Kianmofrad F, Ghafoori E, Elyasi MM, Motavalli M, Rahimian M. Strengthening of metallic beams with different types of pre-stressed un-bonded retrofit systems. Compos Struct 2017;159:81–95.
[21] Hosseini A, Ghafoori E, Motavalli M, Nussbaumer A, Zhao XL, Al-Mahaidi R. Flat prestressed unbonded retrofit system for strengthening of existing metallic I-girders. Compos Part B 2018;155:156–72.
[22] Hosseini A, Ghafoori E, Motavalli M, Nussbaumer A, Zhao X-L. Mode I fatigue crack arrest in tensile steel members using prestressed CFRP plates. Compos Struct 2017;178:119–34.
[23] Hosseini A, Ghafoori E, Motavalli M, Nussbaumer A, Zhao X-L, Koller R. Prestressed unbonded reinforcement system with multiple CFRP plates for fatigue strengthening of steel members. Polymers 2018;10(3):264.
[24] El-Tahan M, Dawood M, Song G. Development of a self-stressing NiTiNb shape memory alloy (SMA)/fiber reinforced polymer (FRP) patch. Smart Mater Struct 2015;24(6).
[25] Izadi MR, Ghafoori E, Motavalli M, Maalek S. Iron-based shape memory alloy for the fatigue strengthening of cracked steel plates: effects of re-activations and loading frequencies. Eng Struct 2018. https://doi.org/10.1016/j.engstruct.2018.09.021. accepted for publication.
[26] Izadi MR, Ghafoori E, Shahverdi M, Motavalli M, Maalek S. Development of an iron-

based shape memory alloy (Fe-SMA) strengthening system for steel plates. Eng Struct 2018;174:433–46.
[27] Ghafoori E, Motavalli M. Innovative CFRP-prestressing system for strengthening metallic structures. J Compos Constr 2015;19(6):04015006.
[28] Ghafoori E, Motavalli M, Nussbaumer A, Herwig A, Prinz G, Fontana M. Determination of minimum CFRP pre-stress levels for fatigue crack prevention in retrofitted metallic beams. Eng Struct 2015;84:29–41.
[29] Ghafoori E, Motavalli M, Nussbaumer A, Herwig A, Prinz GS, Fontana M. Design criterion for fatigue strengthening of riveted beams in a 120-year-old railway metallic bridge using pre-stressed CFRP plates. Compos Part B: Eng 2015;68:1–13.
[30] Ghafoori E, Prinz GS, Mayor E, Nussbaumer A, Motavalli M, Herwig A, et al. Finite element analysis for fatigue damage reduction in metallic riveted bridges using pre-stressed CFRP plates. Polymers 2014;6(4):1096–118.
[31] Ghafoori E, Motavalli M. A retrofit theory to prevent fatigue crack initiation in aging riveted bridges using carbon fiber-reinforced polymer materials. Polymers 2016;8:308.
[32] Ghafoori E, Motavalli M, Zhao XL, Nussbaumer A, Fontana M. Fatigue design criteria for strengthening metallic beams with bonded CFRP plates. Eng Struct 2015;101:542–57.
[33] https://www.vicroads.vic.gov.au. [Accessed 15 May 2018].
[34] Budynas RG, Nisbett JK. Shigley's mechanical engineering design. New York: McGraw-Hill; 2008.
[35] Feltrin G, Jalsan KE, Flouri K. Vibration monitoring of a footbridge with a wireless sensor network. JVC/J Vibrat Control 2013;19(15):2285–300.
[36] Flouri K, Saukh O, Sauter R, Jalsan KE, Bischoff R, Meyer J, et al. A versatile software architecture for civil structure monitoring with wireless sensor networks. Smart Struct Syst 2012;10(3):209–28.
[37] Feltrin G, Popovic N, Flouri K, Pietrzak P. A wireless sensor network with enhanced power efficiency and embedded strain cycle identification for fatigue monitoring of railway bridges. J Sens 2016;2016.
[38] Meteorology A.G.B.o. <http://www.bom.gov.au/climate/current/annual/vic/melbourne.shtml>. [accessed on 25.05.2018].
[39] Noll CJ, Lipson C. Allowable working stress. Soc Exp Stress Anal 1946;3(2):29.
[40] Mischke CR. Prediction of stochastic endurance strength. Trans ASME, J Vibrat, Acoust, Stress Reliab Des 1987;109(1).
[41] Kiguel R. A relation between theoretical stress concentration factor and fatigue notch factor deduced from the concept of highly stressed volume. ASTM Proc 1961;61:73–748.
[42] Brandes EA. Smithells metal reference book. 6th ed. London: Butterworth; 1983.
[43] Haugen EB, Wirsching PH. Probabilistic design. Mach Des 1975;47(12):10–4.
[44] HBM. <https://www.hbm.com/en/6725/article-temperature-compensation-of-strain-gauges/>. accessed on 24.04.2018.
[45] Ahmed A, Tavakol B, Das R, Joven R, Roozbehjavan P, Minaie B. Study of thermal expansion in carbon fiber reinforced polymer composites. In: Proceedings of SAMPE international symposium. Charleston, SC; 2012.
[46] Wikipedia. <https://en.wikipedia.org/wiki/Thermal_expansion> [accessed on 25.04.2018].